Naval Research Laboratory
Washington, DC 20375-5320

NRL/MR/6721--93-7347

Temperature Diagnosis of Ion-Beam-Driven Foam Targets Using K Shell Features from Trace Elements

JOHN P. APRUZESE
JOHN E. ROGERSON
ROBERT W. CLARK

Radiation Hydrodynamics Branch
Plasma Physics Division

MARGARET C. COULTER

Berkeley Research Associates
Springfield, VA

September 3, 1993

REPORT DOCUMENTATION PAGE

Form Approved
OMB No. 0704-0188

1. AGENCY USE ONLY (*Leave Blank*)	2. REPORT DATE	3. REPORT TYPE AND DATES COVERED
	September 3, 1993	Final

4. TITLE AND SUBTITLE

Temperature Diagnosis of Ion-Beam-Driven Foam Targets Using K Shell Features from Trace Elements

5. FUNDING NUMBERS

PE - 63220C

6. AUTHOR(S)

John P. Apruzese, John E. Rogerson, Robert W. Clark, and Margaret C. Coulter

7. PERFORMING ORGANIZATION NAME(S) AND ADDRESS(ES)

Naval Research Laboratory
Washington, DC 20375-5320

8. PERFORMING ORGANIZATION REPORT NUMBER

NRL/MR/6721--93-7347

9. SPONSORING/MONITORING AGENCY NAME(S) AND ADDRESS(ES)

Sandia National Laboratories
Albuquerque, NM 87175-5800

10. SPONSORING/MONITORING AGENCY REPORT NUMBER

11. SUPPLEMENTARY NOTES

This work was performed by the Radiation Hydrodynamics Branch, Plasma Physics Division for Sandia National Laboratories under contract No. DC-AC04-76DP00789, purchase order AB-8449.

12a. DISTRIBUTION/AVAILABILITY STATEMENT

Approved for public release; distribution unlimited.

12b. DISTRIBUTION CODE

13. ABSTRACT (*Maximum 200 words*)

This report describe a practical method of diagnosing the temperature achieved in foam targets driven by energetic ion beams. The hydrocarbon foams are doped with NaF at a density of 6×10^{18} cm^{-3}. Together with the carbon, and possibly oxygen, present in the foam, the K shell ionization stages of thee elements change distinctly in their spectroscopic features as the foam temperature increases from 50 to 200 eV. A full radiation-hydrodynamics simulation of an x-ray driven magnesium plasma is also described and compared with experimental data.

14. SUBJECT TERMS

Ion beam fusion
Radiation transport
Tracer elements
X-ray spectroscopy
Temperature diagnosis
Radiation hydrodynamics

15. NUMBER OF PAGES

42

16. PRICE CODE

17. SECURITY CLASSIFICATION OF REPORT	18. SECURITY CLASSIFICATION OF THIS PAGE	19. SECURITY CLASSIFICATION OF ABSTRACT	20. LIMITATION OF ABSTRACT
UNCLASSIFIED	UNCLASSIFIED	UNCLASSIFIED	UL

CONTENTS

Executive Summary

The work reported in this document establishes the theoretical feasibility of a straightforward and practical spectroscopic method for determining the temperature of ion beam target plasmas derived from hydrocarbon foams. The technique is most appropriately applied to the time frame following the passage of the ion beam, when direct beam excitation of the atomic states of the target material has ceased. For the temperature range of 50-200 eV, it is found that uniformly doping the foam with NaF and/or oxygen, each at atomic densities of about 6×10^{18} cm^{-3}, will result in the production of characteristic K shell x-ray features from these elements. For reasons discussed in the text, many of the spectral lines are predicted to appear in absorption. The temperatures are primarily differentiated by the presence or absence of various lines from the six K shell ionization stages of these three elements. Some of the lines would be seen in emission in the upper part of the temperature range considered. This phenomenon also is useful as a temperature indicator. Using dopants of different density or atomic number than those given above has also been considered, but detailed calculations have shown such approaches to be less than optimum. For very low density foams in which doping is not practical, the use of a foam containing oxygen is recommended as our calculations show that the oxygen lines may potentially contain diagnostic information which is difficult to obtain from carbon alone.

We have also carried out a full radiation-hydrodynamic simulation of an experiment at Sandia National Laboratories in which a Z pinch x-ray source heated a 1 μm thick "macrodot" of MgF_2. The MgF_2 gradually heats and expands and near the peak of the radiation pulse reaches temperatures of 70-80 eV and electron densities of $(1\text{-}4) \times 10^{20}$ cm^{-3}. These values are consistent with previous estimates at Sandia using line ratios, indicating that a good understanding of the experiment has been achieved.

TEMPERATURE DIAGNOSIS OF ION-BEAM-DRIVEN FOAM TARGETS USING K SHELL FEATURES FROM TRACE ELEMENTS

I. Introduction

In evaluating the performance of pulsed-power-driven targets, the need to determine their temperature frequently arises. This is particularly true for foam converters used in inertial confinement fusion (ICF) driven by light ion beams. At Sandia National Laboratories, the Particle Beam Fusion Accelerator II (PBFA II) deposits ion energy into a low-density hydrocarbon foam target for the purpose of converting this energy to copious x radiation to drive a fuel capsule. This indirect drive method, aimed ultimately at achieving breakeven and beyond, requires optimum and well understood performance from the foam plasma radiation converter.

A key parameter in determining the radiation temperature and spectrum is the electron temperature of the ion-beam-driven foam plasma. In addition to being one of the benchmarks of converter performance, the foam plasma temperature is also an important indicator of how well the ion beam has coupled to the target. Many of these issues are discussed in greater detail elsewhere[1]. As indicated in Ref. 1, many diagnostic instruments have been successfully deployed in the difficult environment of the PBFA II pulsed ion accelerator, among them several spectrographs and x-ray diodes. However, some useful diagnostic techniques, such as laser-driven target backlighting, are not currently feasible in PBFA II experiments due to cost and space limitations. The purpose of this report is to assess in detail a flexible yet simple and accurate method that makes use of conventional x-ray spectroscopy and is practical for PBFA II targets. In this approach, the hydrocarbon foam converters are doped with trace amounts of elements (O, F, Na) which absorb or radiate different K shell features from different ionization stages as the temperature changes. We emphasize that the presently described techniques apply to the target after the passage of the energizing ion beam, therefore the spectral responses due to direct excitation of atomic levels by the ion beam are not modeled.

In the succeeding sections this technique is evaluated in detail for a variety of expected target conditions. Sec. II describes the NRL model for coupled atomic physics and radiation in a plasma, and compares our calculated opacities to both the XSN and Los Alamos values for parameters relevant to expected PBFA II conditions. In Sec. III we discuss the basic radiation physics which underlies the formation of the principal x-ray features, whether emission or absorption. Sec. IV presents results for homogeneous doped foams with both temperature and density varying or with

Manuscript approved May 20, 1993.

fixed density and variable temperature. Sec. V discusses inhomogeneous foam plasmas, and in Sec. VI, a full radiation-hydrodynamic simulation of the MgF_2 "macrodot" experiment carried out on the Sandia pulsed power accelerator, Saturn, is presented.

II. Model and Opacity Comparison

The results presented below were obtained with a plasma model which has been in use for some time at the Naval Research Laboratory and is extensively documented in the literature. This model employs detailed configuration structures of various atomic ions and their associated coupling rates and solves for the self-consistent level populations and radiation field (both internal and emitted) in a specified plasma. Radiative transfer is calculated using either a cell-to-cell coupled escape probability technique or full multifrequency treatment. Due to the significant line-continuum interactions in the ion beam target plasmas analyzed in the present work, multifrequency transport was employed. Various assumptions can be invoked in exercising the model, namely Local Thermodynamic Equilibrium (LTE), Collisional Radiative Equilibrium (CRE), or the full time-dependent rate equations can be integrated. The latter, obviously more expensive approach is usually reserved for cases where the atomic physics and radiation are coupled to a hydrodynamic simulation (see Ref. 2, for example). The full multifrequency transport option has been employed in previous instances where ICF targets (laser-driven capsules) were investigated. The NRL model obtained excellent agreement with experimentally observed x-ray spectra for implosions of neon-filled microballoons at the University of Rochester (Ref. 3) and DT-argon filled spherical targets at Los Alamos National Laboratory (Ref. 4).

In the targets considered in this work several elements are present. In addition to the carbon and hydrogen of the foam, dopants (O, F, and Na) are used as tracer temperature diagnostics. A separate data table is consulted for each element; energies of levels and radiative rates are obtained from various literature sources or Cowan's atomic structure code. Collisional and photoionization rates are from distorted wave or semiclassical calculations, or previously published sources, as appropriate. We aim to include all important atomic processes coupling the modeled levels, such as electron collisional excitation and de-excitation, radiative, 3-body and dielectronic recombination, collisional and photoionization, bound-bound radiative decay and photoexcitation. In solving the radiative transfer equation, the opacity at each of approximately 2600 frequencies is obtained by

adding the absorption coefficients from bound-bound, bound-free, and free-free radiative processes for each of the elements in the plasma. This generates the internal radiation field for calculation of photoexcitation and photoionization rates as well as the emitted spectrum for comparison with experimental data. A Voigt profile is assumed for each of the spectral lines, with the broadening parameter obtained from the radiative and collisional lifetimes of the upper and lower levels of the transition in question. Further details regarding the rates may be found in Ref. 5.

For the dopants, O, F, and Na, as well as Mg which is needed for a separate simulation, the atomic models used are analogous for isoelectronic sequences. Excited state structure is included for the lithiumlike, heliumlike, and hydrogenic ions through n=5. The hydrogenic levels are differentiated by principal quantum number only. For the heliumlike stage, the structure is broken into individual singlet and triplet sublevels through n=3, and treated as single Rydberg levels by principal quantum number only for higher-lying states. In the lithiumlike sequence, the levels are broken out by both principal and orbital quantum number through n=3, and for n=4 and 5, only by principal quantum number. For carbon a somewhat simpler model is sometimes used which includes states only through n=2 for the K shell. This reduces cost and storage, and does not sacrifice essential accuracy because the electron densities considered are generally sufficient to force LTE populations for carbon but not for the higher Z dopants, as discussed below in the next section. The accuracies of the opacities given by this carbon model are demonstrated below in a comparison with other models. Note that the hydrogen is nearly always fully ionized and does little other than contribute electrons and add some mass. It is, however, modeled with a small atomic data table containing the neutral ground and bare nuclear stages.

Our model generates opacities comparable to those obtainable from two widely employed data bases, the XSN model[6], developed at Lawrence Livermore National Laboratory, and the Los Alamos opacities[7]. We have chosen conditions for comparison which are typical of those used in our foam model calculations. The mass density is 20 mg cm^{-3} of CH, corresponding to an atomic density of 9.3×10^{20} cm^{-3}. The electron temperature is 100 eV. Fig. 1 presents a direct comparison of the detailed spectral opacities predicted by the three models. Note the general agreement across the spectrum extending from 10 eV to 10 keV. Minor differences are largely due to the presence or absence of specific lines and their assumed profiles. Note that the opacity is given in cm^2 g^{-1}, easily convertible to absorption coefficient in cm^{-1} by multiplying by the density, in this case 0.02

NRL

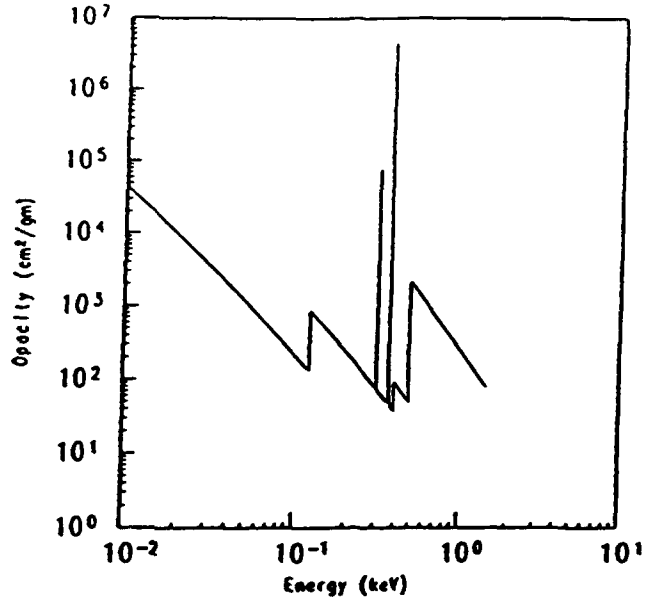

XSN

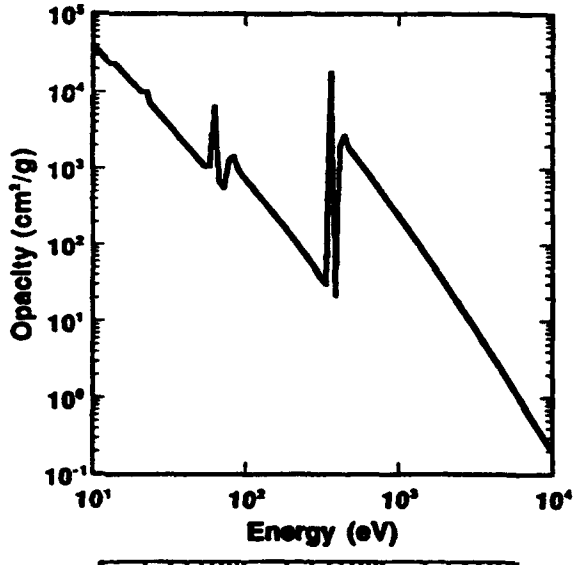

LANL

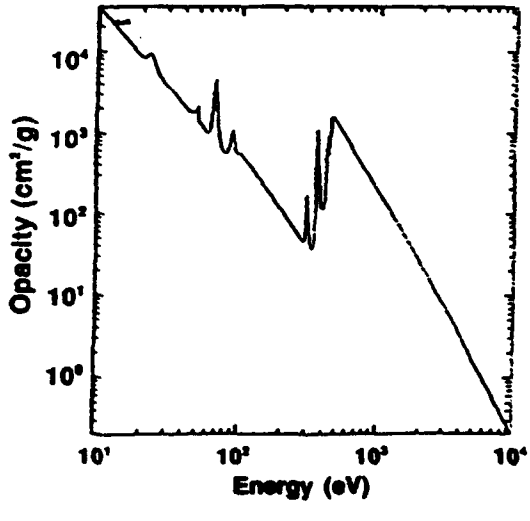

FIG. 1. Opacity in $cm^2\ g^{-1}$ is plotted against energy from 10 eV to 10 keV for CH at an electron temperature of 100 eV and mass density of 20 mg cm^{-3}. The results of three different models, NRL, XSN, and LANL, are shown for comparison.

g cm^{-3}. At energies below 100 eV, free-free absorption dominates the opacity, whereas above this value, bound-free transitions are the principal contributor. In oxygen-free foams, carbon is the principal source of opacity, and this comparison demonstrates that our model can accurately characterize this critical parameter in the regime of interest.

III. Relevant Radiation Physics

The purpose of this section is to describe the physical principles which explain the specific results presented in the succeeding sections. Those results suggest observable spectroscopic features as diagnostic tools for the conditions of the target plasma. Therefore we ask the basic question: what governs the formation of x-ray spectra in the types of target plasmas of interest?

For a plasma to radiate as a blackbody two conditions must be met. First, the plasma must be optically thick in the spectral region being considered, and, second, the level populations which do the radiating must be distributed according to the Saha-Boltzmann equation. The first of these conditions is straightforward and easily understood. One simply multiplies the absorption coefficient by the thickness of the plasma. We consider foam plasmas 0.5 cm thick for most of the cases run in this study. The optical depth for the conditions of Fig. 1, for example, may be obtained by multiplying the opacity in cm^2 g^{-1} by the density (0.02 g cm^{-3}) and the 0.5 cm thickness, for any photon energy of interest. When this is done for Fig. 1, it is found that the optical depth exceeds unity except for a small region of energies near 400 eV, and even there, the optical depth is a few tenths or so. Therefore, a CH foam of density 20 mg cm^{-3} has the potential to radiate a near-Planckian spectrum over a large region of the soft x-ray spectrum, if its populations are in LTE, which we now consider.

For a Saha-Boltzmann (LTE) population distribution to prevail, the particle distribution must be Maxwellian, which we assume throughout this work, and the collision rates produced by those particles must well exceed the corresponding radiative decay rates. We confine our discussion to the K shell ionization stages, for which the spontaneous decay rates vary as Z^4 (Ref. 8), where Z is the atomic number. The collisional rates vary as $N_e Z^{-3}$ (Ref. 9), therefore to maintain a fixed ratio of collisional to radiative rates required for LTE means that the electron density must scale as Z^7. Clearly, it is much easier to bring the K shell into LTE for low atomic number elements. The detailed investigation of Ref. 10 found that for optically thin Al (Z = 13), an

electron density of about 10^{25} is needed to force the K shell stages into LTE. The electron density required for LTE, assuming Z^7 scaling, is plotted in Fig. 2 for atomic numbers $6 \leq Z \leq 13$. Note that LTE for K shell carbon requires an electron density of $\sim 5 \times 10^{22}$ cm^{-3}, about an order of magnitude higher than that obtained at a foam density of 20 mg cm^{-3}. However, virtually all of the principal resonance transitions are optically thick at this density for a half centimeter foam. The resulting self-absorption in the lines greatly reduces the effective decay rate, thus the electron density needed for LTE populations is effectively lowered to values close to those attained. It is therefore reasonable to expect carbon to be fairly close to LTE. However, Na, one of the dopants considered, requires a density $\sim (11/6)^7 \sim 70$ times that of C and therefore should not be expected to be nearly as close to LTE.

To illustrate this point and also show why absorption lines are prevalent in much of the results that follow, consider the excitation of the principal heliumlike resonance line of Na at its energy E of 1127 eV. This is a very strong transition with an oscillator strength, f, of 0.75. For photoexcitation, assume that the sodium ion is in the interior of the foam and sees a 100 eV Planckian spectrum over all 4π steradians. The photoexcitation rate P is given by

$$P(sec^{-1}) = \int \frac{4\pi B_\nu(T)}{h\nu} \sigma_\nu d\nu \qquad (1)$$

where σ_ν is the line cross section in cm^2, whose frequency integral is $\frac{\pi e^2}{mc} f$. Using the excellent approximation that the Planck function is constant over the narrow spectral line profile leads to

$$P = \frac{4.34 \times 10^7 E^2(eV)}{e^{E/kT} - 1} f. \qquad (2)$$

Eq. (2) yields a line photoexcitation rate of 5.27 x 10^8 sec^{-1} for the sodium He α line immersed in a 100 eV blackbody. At the surface of the foam plasma, the ambient radiation field is reduced by at least a factor of 2 due to geometry alone. Greater reductions are possible due to line self-absorption (see Ref. 11). By contrast, the collisional excitation rate of the upper level of this line at 100 eV and electron density of 5 x 10^{21} cm^{-3} is just 6 x 10^6 sec^{-1}. Accordingly, it is expected that the upper level populations of the dopants may be dominated by photoexcitation and thus be reduced near the boundaries of the foam. Since many of their K shell lines are optically thick, this has the consequence that they may be seen in absorption against a background of near-Planckian continuum radiation. This is predicted to be the case quite often, as seen in the following section.

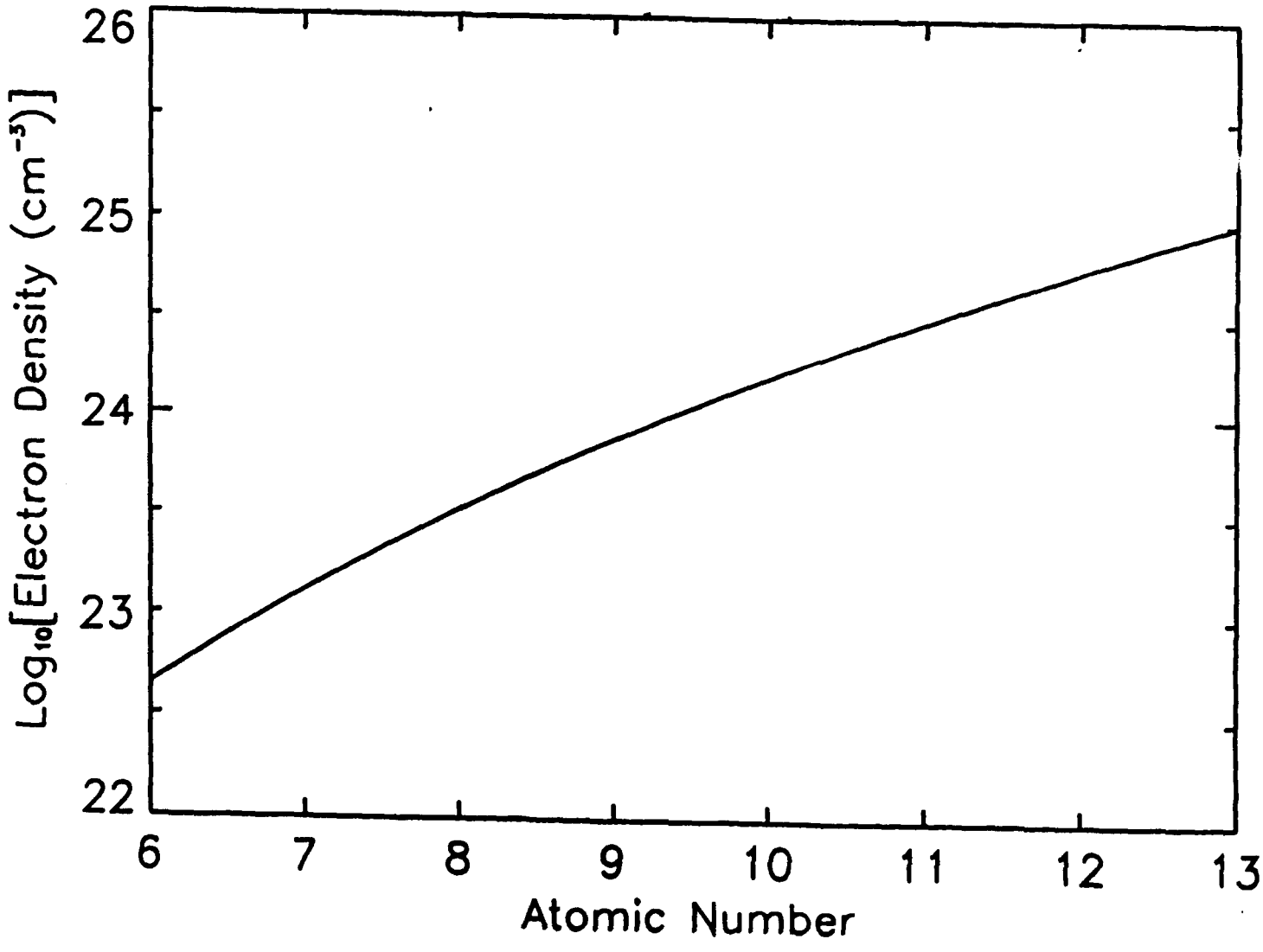

FIG. 2. Approximate electron density required for LTE in an optically thin, K shell dominated plasma is plotted vs. atomic number.

IV. Homogeneous Doped Hydrocarbon Foam Plasmas

The following subsections report the results of detailed calculations in which trace amounts of elements of similar atomic number are assumed doped into the foam target. A similar technique has been used with considerable success at the University of Rochester[12] to diagnose the temperature of laser-imploded spherical targets. The advantages of this method are discussed in Ref. 12. An important point is that the functional forms of the temperature and atomic number dependences of the various rate coefficients are well known. Even though the absolute values of the rates may contain significant errors and uncertainties, in taking their ratios from two elements of nearby atomic number, those errors generally cancel to first order. This is especially true for the well-known atomic physics of the K shell, to which we confine our analysis. In the temperature regime of interest for PBFA II experiments, elements with atomic number above sodium (Z=11) are only weakly excited in the K shell. The most promising diagnostic tracers were found to be F and Na (which presumably can be easily doped as NaF) as well as O, which can also be present as integral to the foam target composition. Neon would probably also be excellent but its status as a noble gas in all likelihood renders its use unfeasible and it was not considered in the present work.

A. Temperature Increase with Density

The initial studies consider foams in which the density and temperature are assumed to increase concurrently. Four specific CH foams were analyzed in detail: assumed temperatures and densities of 50 eV and 10 mg cm^{-3}, 100 eV and 20 mg cm^{-3}, 150 eV and 30 mg cm^{-3}, and a 200 eV foam with an assumed density of 40 mg cm^{-3}. Calculations were run in which uniform doping with NaF at various densities was assumed, and also in which a solid-density layer of NaF was placed on one side of the foam.

The most promising configuration was found to be uniform doping at a concentration of 6 x 10^{18} atoms cm^{-3} of both Na and F. An extensive series of computations at lower densities showed that no additional diagnostic insights were obtained, but the characteristic features were weakened and therefore more difficult to detect. At 6 x 10^{18} cm^{-3}, the mass density of NaF is 0.4 mg cm^{-3}, unlikely to affect the hydrodynamics of the foams which are well over an order of magnitude more dense. However, at an order of magnitude higher dopant concentrations, the NaF mass density

would be an appreciable fraction of the foam density and thus perturb its behavior.

In calculations in which a contiguous solid density layer of NaF is present, the electron density of about 3×10^{23} cm^{-3} greatly enhances the 3-body recombination rate, making it much harder to ionize these elements to the K shell. These two elements are also much closer to LTE than at dopant densities. Therefore, there is a nearly LTE solid layer radiating against a nearly Planckian continuum produced by the carbon in the foam. Not surprisingly, the features which are present are very weak and of little diagnostic value. The specific results of the most promising configuration, namely, the uniform NaF doping at 6×10^{18} cm^{-3}, are now considered.

Figures 3-6 present the region of the spectrum from 0.7 to 1.7 keV, as calculated to be emitted by an 0.5 cm thick foam at temperatures of 50, 100, 150, and 200 eV, at CH densities of 10, 20, 30, and 40 mg cm^{-3}, respectively. Uniform doping of NaF at a density of 6×10^{18} cm^{-3} is assumed in each case. One quite attractive feature of using NaF is that their K shell lines are cleanly separated, all of the F lines lying below 1100 eV and the Na lines being above this energy. Note from Figs. 3-6 that most of the lines appear in absorption, for reasons discussed above in Sec. III. The results show that the various temperatures can be distinguished experimentally by mostly obvious qualitative features of the spectra. In each figure the dashed line is the blackbody spectrum for the calculated temperature shown for comparison. The distinguishing characteristics:

- 50 eV: Only the He-like lines of F are evident, all in absorption.
- 100 eV: Both the He-and H-like lines of F are seen in absorption; for Na, only the He-like lines are seen, all in absorption.
- 150 eV: Both He-and H-like lines of Na are now seen in absorption: both species of F are still visible. A hint of emission appears in the wings of some of the higher lines in Na.
- 200 eV: The Lyman lines of F arising from $n > 2$ and all lines of Na for $n > 2$ are now seen in emission.

These calculations establish clear benchmarks for determining the foam temperature with $\sim$ 50 eV resolution from 50 to 200 eV, when the density increases along with the temperature. It is of interest to also determine how well one can resolve the temperature spectroscopically with this technique, and also if increasing the temperature at a fixed density leads to significant quantitative

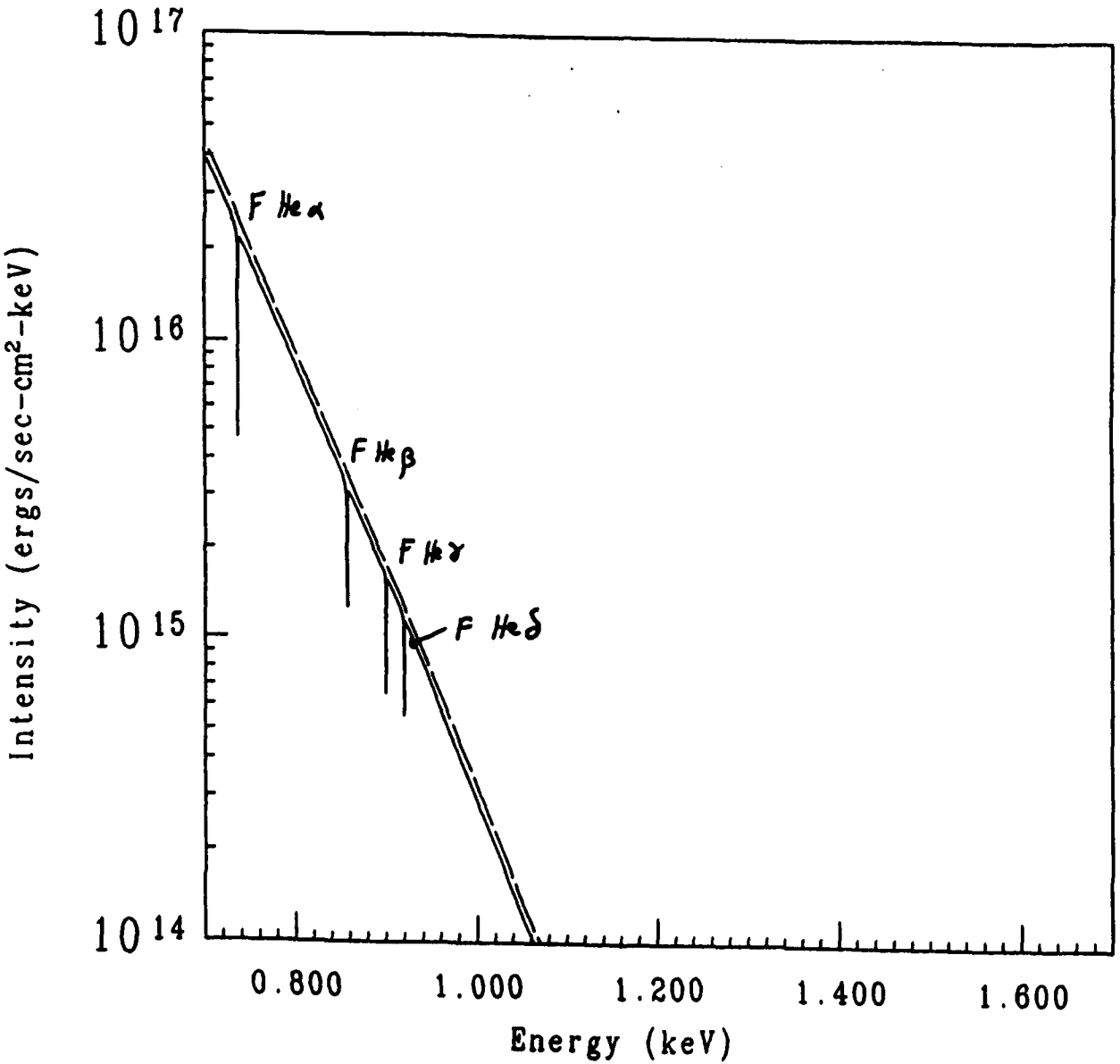

FIG. 3. Emitted spectrum as calculated to arise from a CH foam plasma of density 10 mg cm^{-3} and temperature 50 eV. The thickness of the foam is 0.5 cm and it is assumed to be doped with NaF at a density of 6×10^{18} cm^{-3}. The dashed line is a 50 eV blackbody spectrum for comparison.

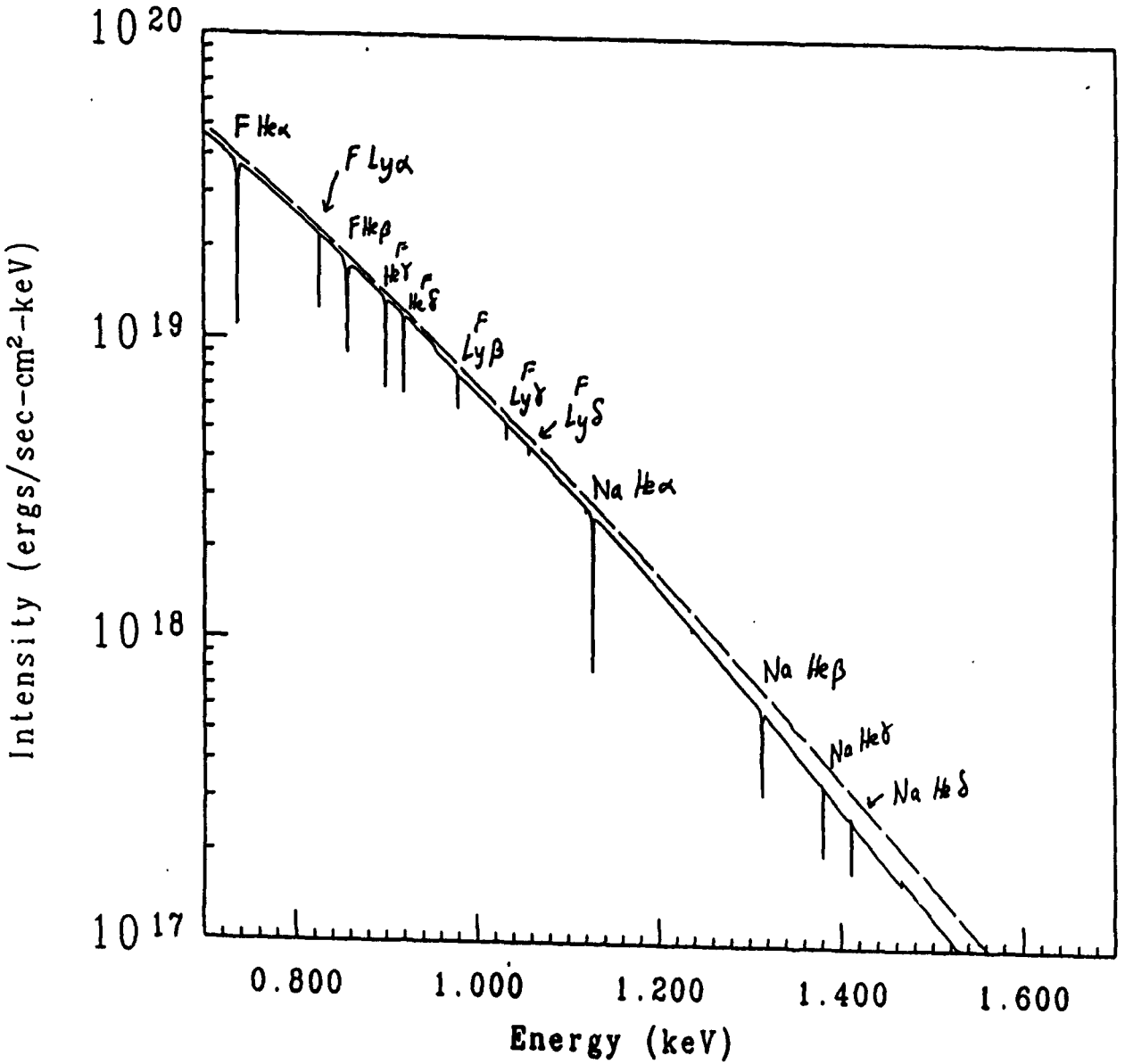

FIG. 4. As in Fig. 3, except that the plasma temperature and density are 100 eV and 20 mg cm^{-3}, respectively.

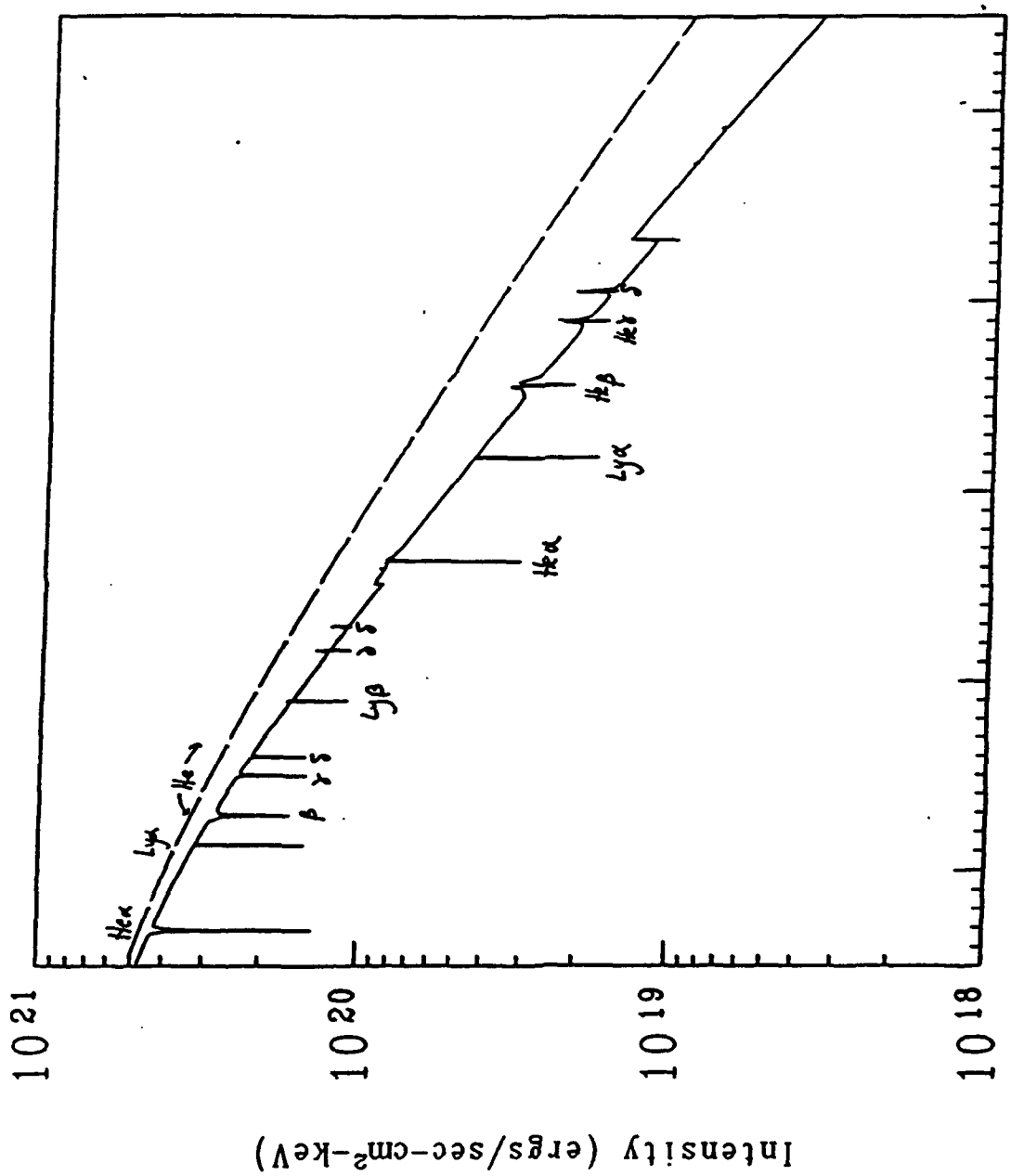

FIG. 5. As in Figs. 3 and 4, except that the temperature and density are 150 eV and 30 mg cm^{-3}.

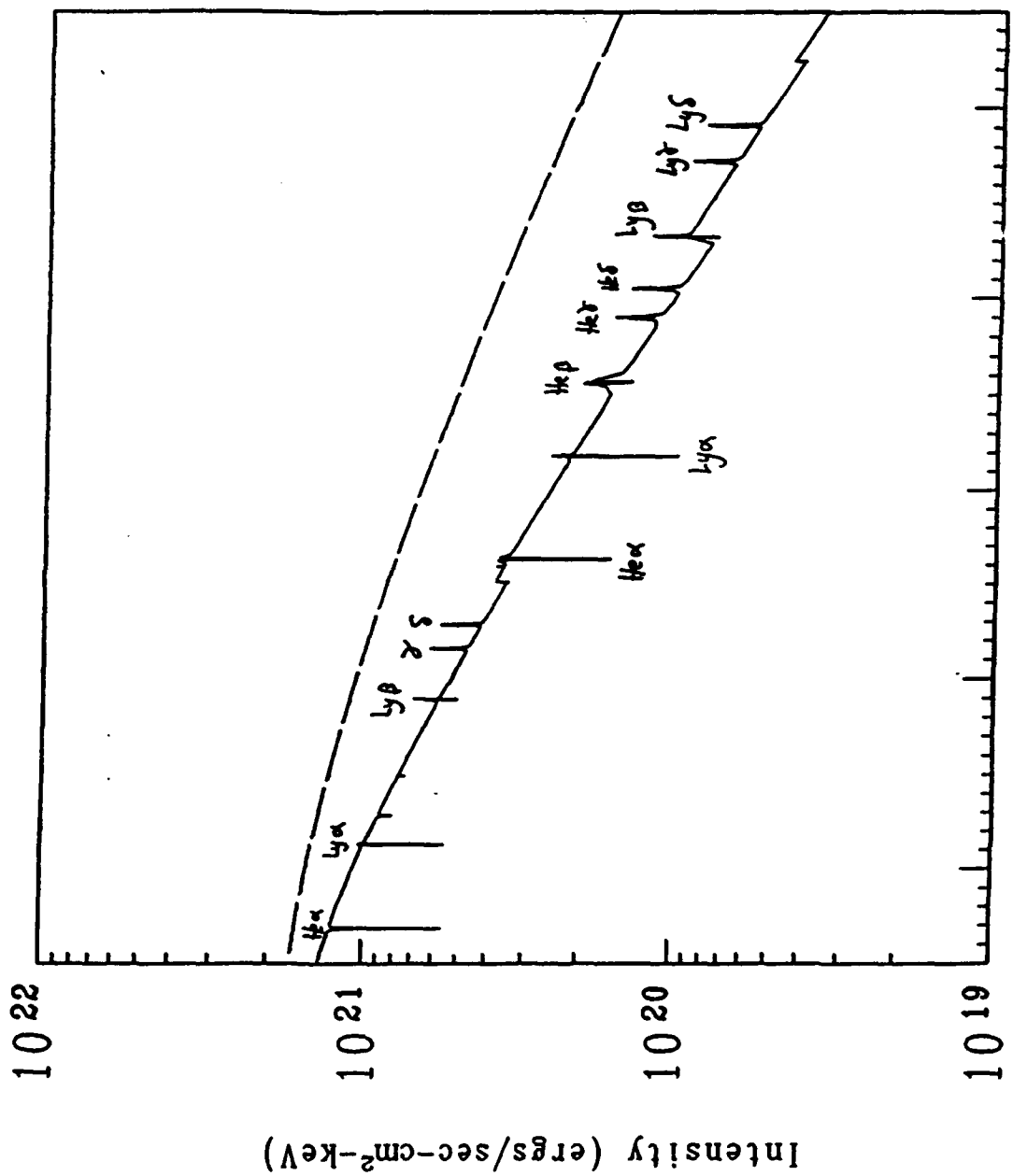

FIG. 6. As in Figs. 3, 4, and 5, except that the temperature and density are 200 eV and 40 mg cm^{-3}.

or qualitative changes.

B. Fixed Density Calculations

The spectra discussed in this section were all calculated assuming a fixed CH foam density of 10 mg cm^{-3}. All dopants are spatially uniform at an atomic density of 6 x 10^{18} cm^{-3}. The temperatures considered are: 50, 60, 70, 80, 90, 100, 120, 140, 150, and 200 eV. The respective spectra appear in Figs. 7-14.

Initial calculations were performed with NaF as the only dopant, as was done in the work discussed in the previous section. Clear and useful diagnostic trends were seen with promising experimental benchmarks for each increment in temperature, *except* for the 60-70 eV interval, where only mild sensitivity was observed in the Na and F spectra. Therefore, an oxygen K shell table was set up, and O was assumed as a dopant (also at an atomic density of 6 x 10^{18} cm^{-3}) for the runs from 50 to 70 eV. For these three spectra, photon energies from 500 to 1500 eV are shown so that the oxygen K shell lines may be included in the plots, whereas the other runs only use Na and F and the spectra are displayed from 700 to 1700 eV. Summarizing the important features:

- 50 eV: Only the He-like lines of both F and O are present, all in absorption.
- 60 eV: The He-like lines of Na now appear.
- 70 eV: The Ly α line of O appears.
- 80 eV: The Ly α line of F appears.
- 90 eV: The higher Lyman series lines of F are now detectable.
- 100 eV: As the temperature increases, the continuum begins to fall away from the Planck limit in the keV region. This causes emission lines to form for the higher series He-like Na lines. The density is half of the 20 mg cm^{-3} assumed in the previous calculation at 100 eV. The emission lines have self-reversed cores.
- 120 eV: The F lines arising from $n \geq 3$ are now in emission.
- 140 eV: F Ly α is now in emission but with a self-reversed core.
- 150 eV: The Ly α line of Na appears with a deep self-reversed core.

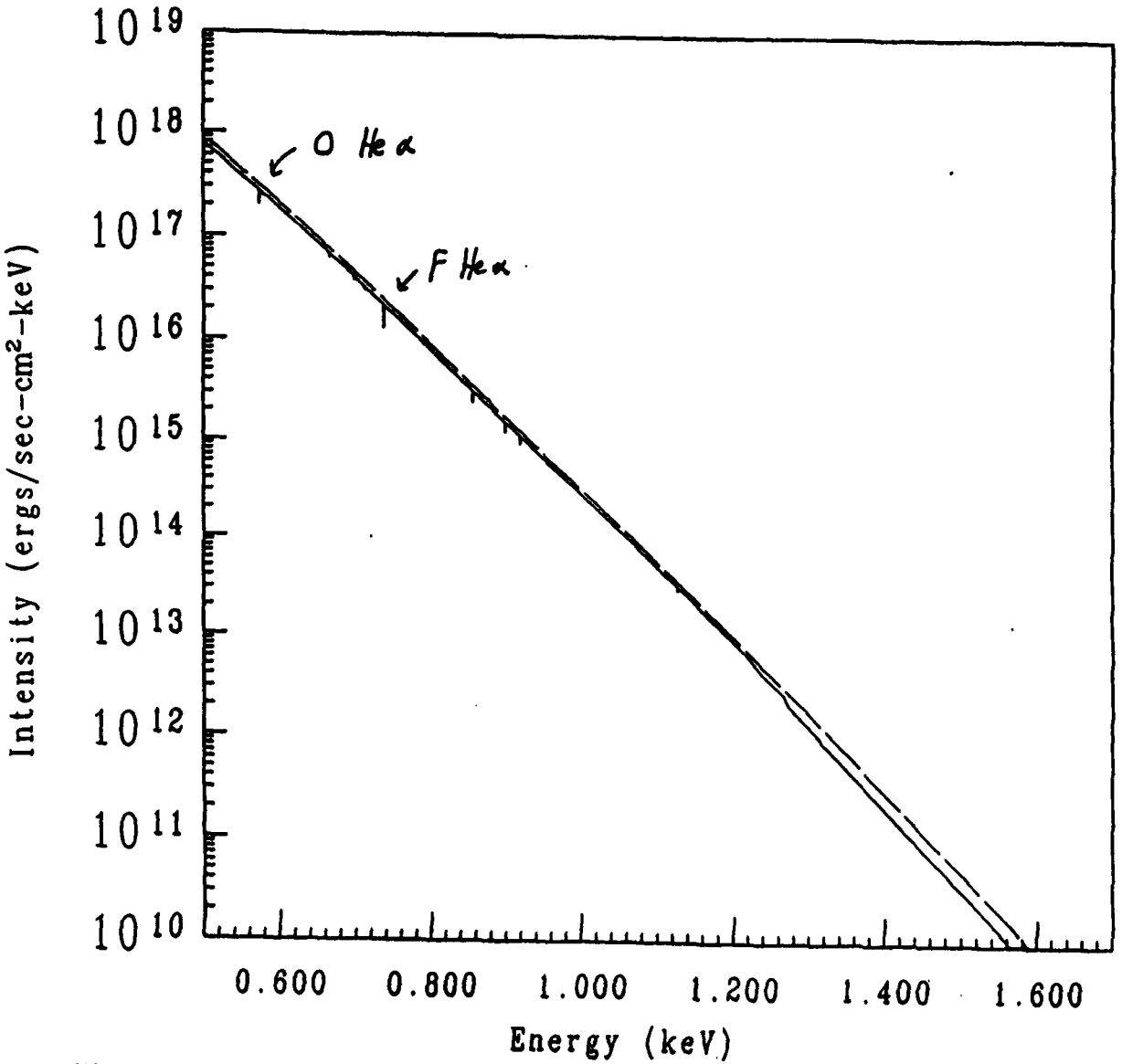

FIG. 7. Emitted spectrum calculated from a CH foam plasma of density 10 mg cm^{-3} and temperature 50 eV. Thickness of the plasma is 0.5 cm and it is uniformly doped with O, F, and Na each at a density of 6×10^{18} cm^{-3}. Dashed line is Planckian at the same temperature for comparison.

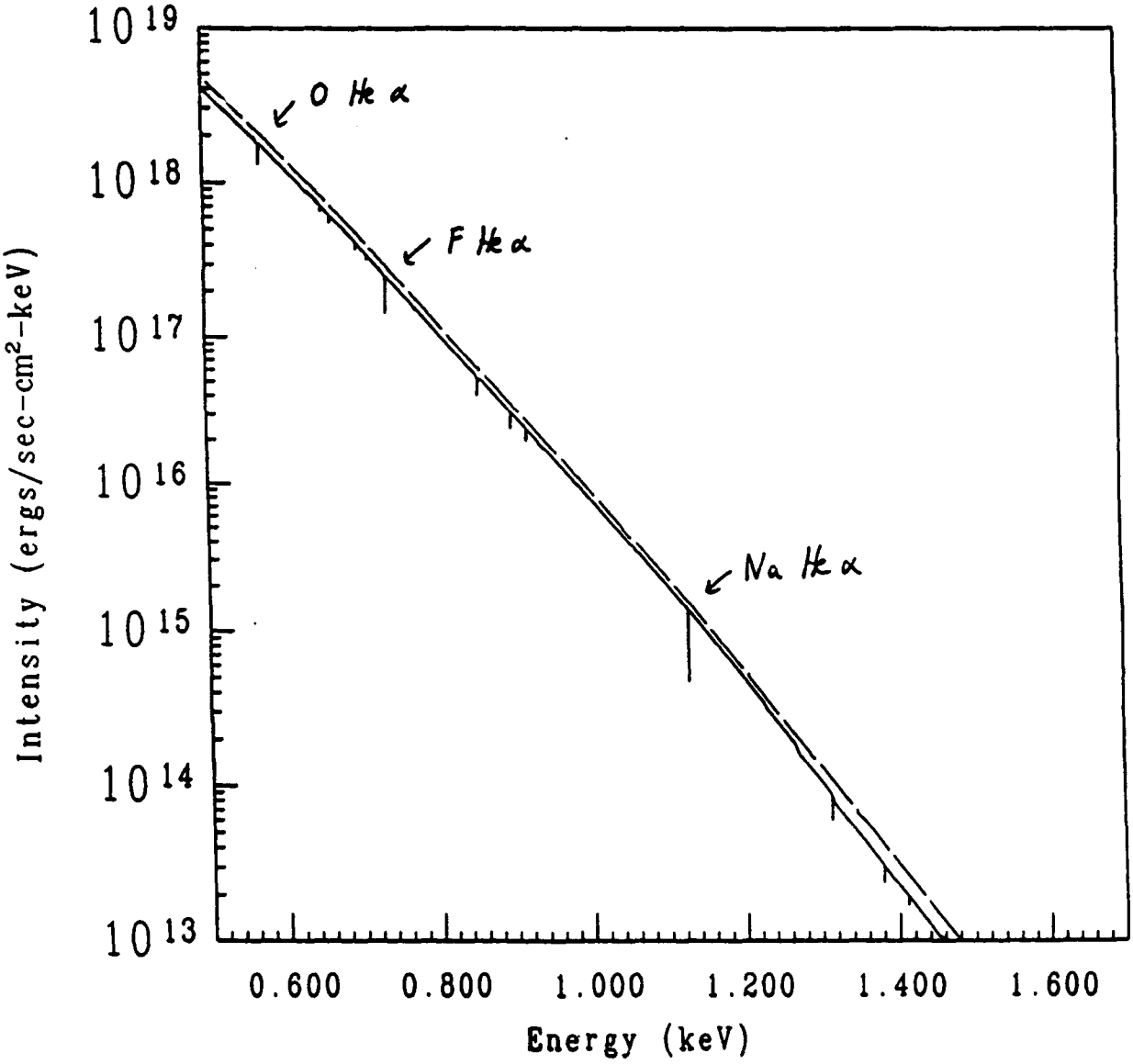

FIG. 8. As in Fig. 7, except that the temperature is 60 eV.

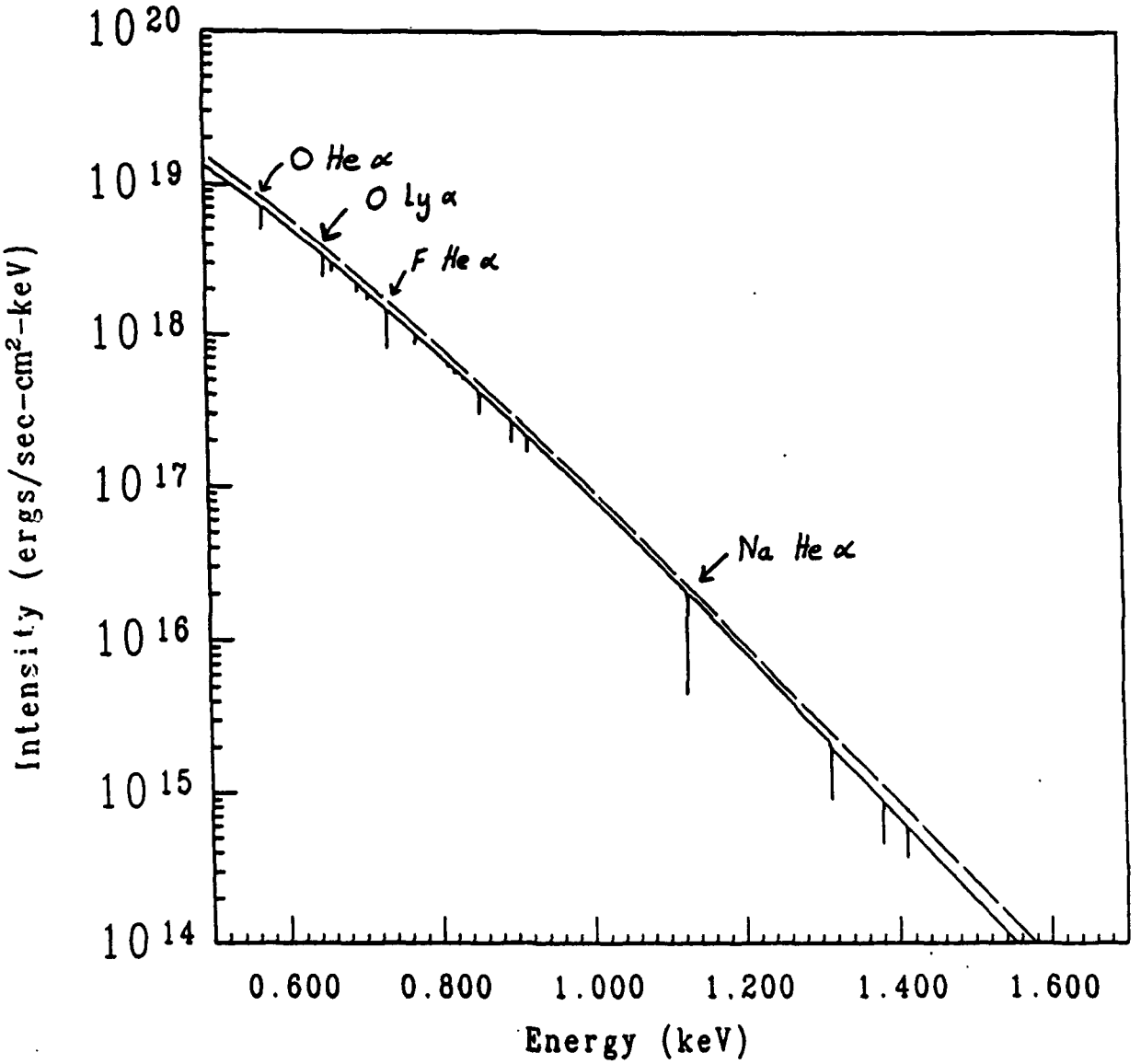

FIG. 9. As in Figs. 7 and 8, except that the temperature is 70 eV.

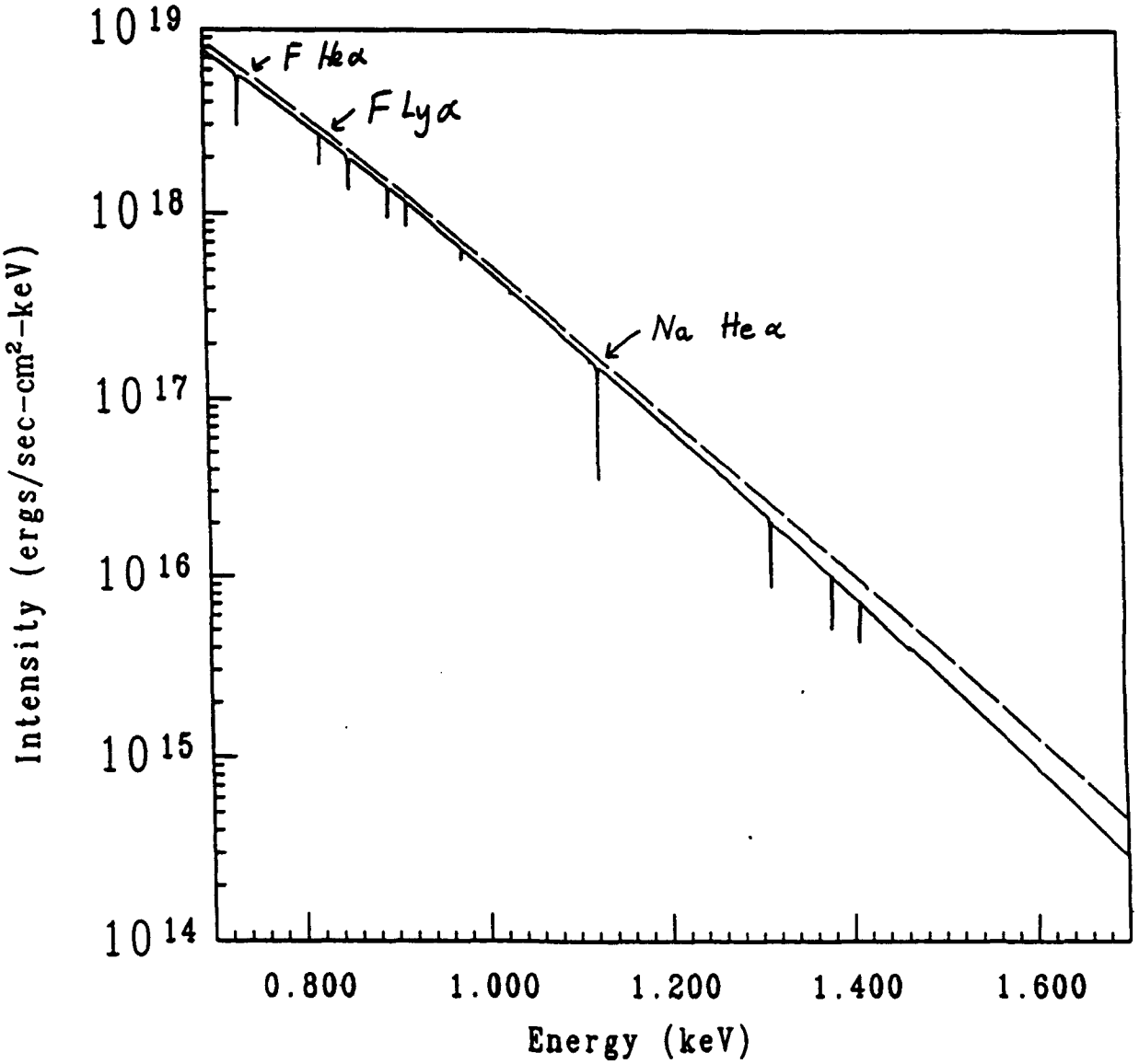

FIG. 10. As in Figs. 7-9, except that only Na and F are used as dopants, and the temperature is 80 eV.

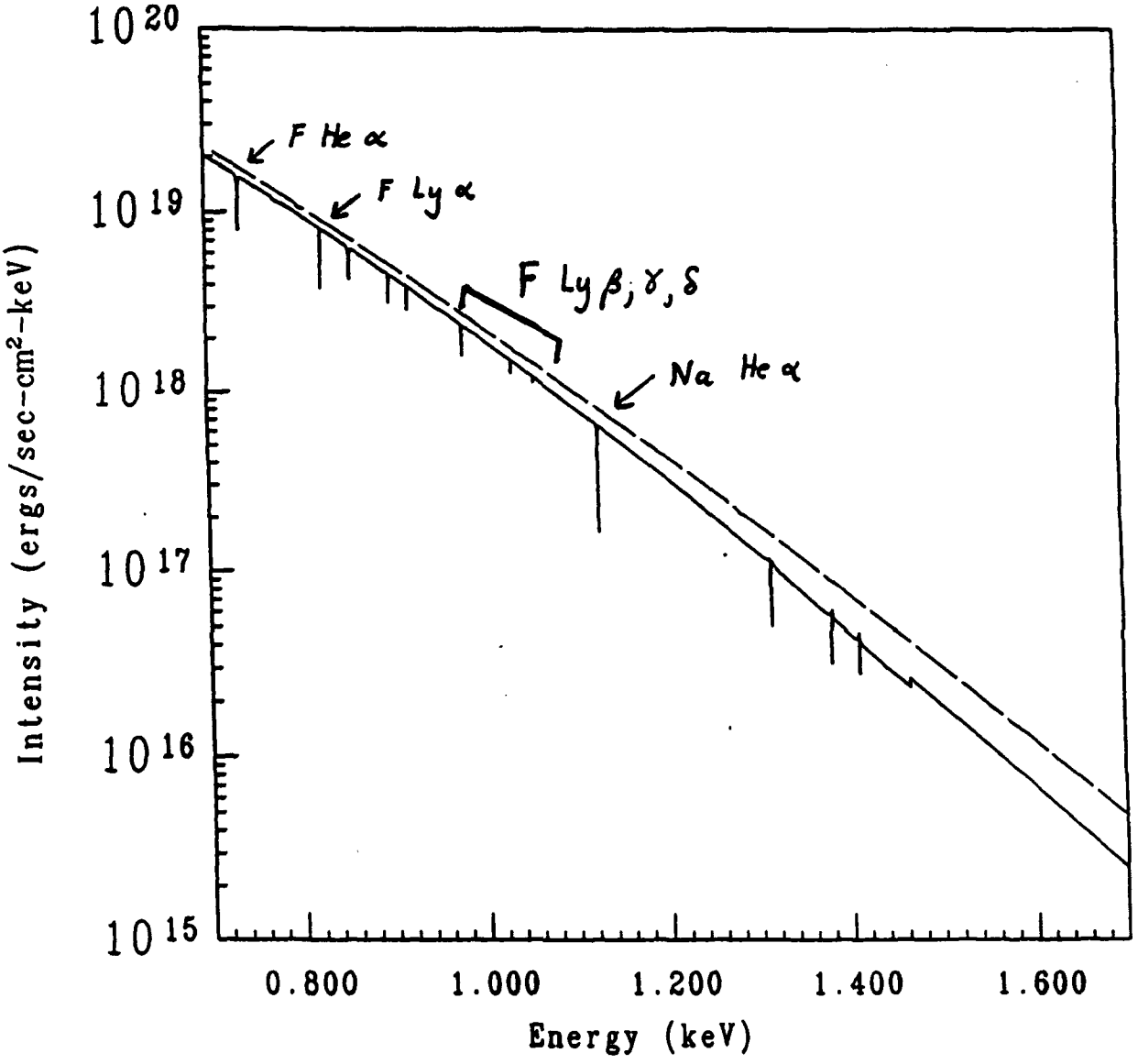

FIG. 11. As in Fig. 10, except that the temperature is 90 eV.

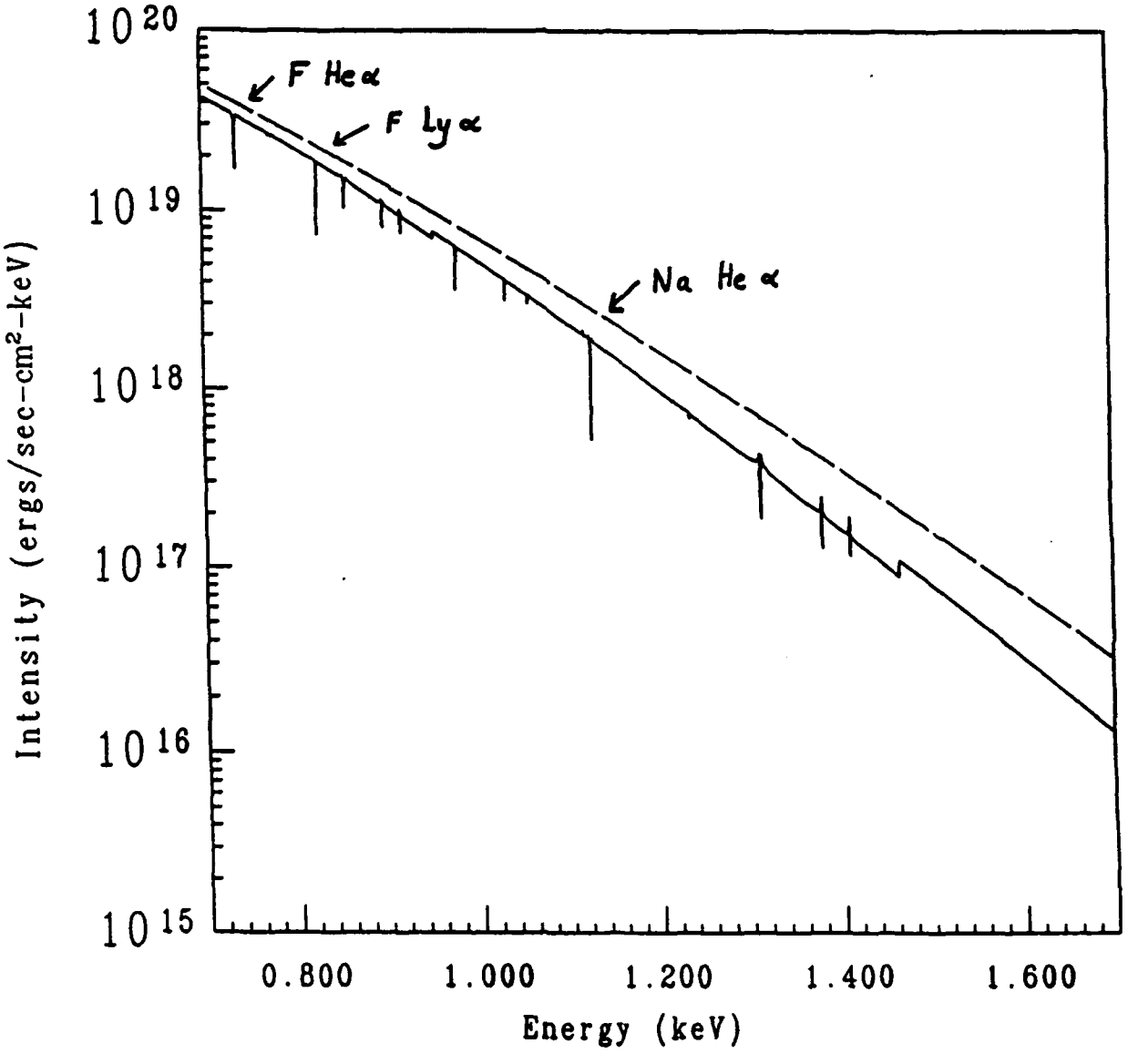

FIG. 12. As in Figs. 10 and 11, except that the temperature is 100 eV.

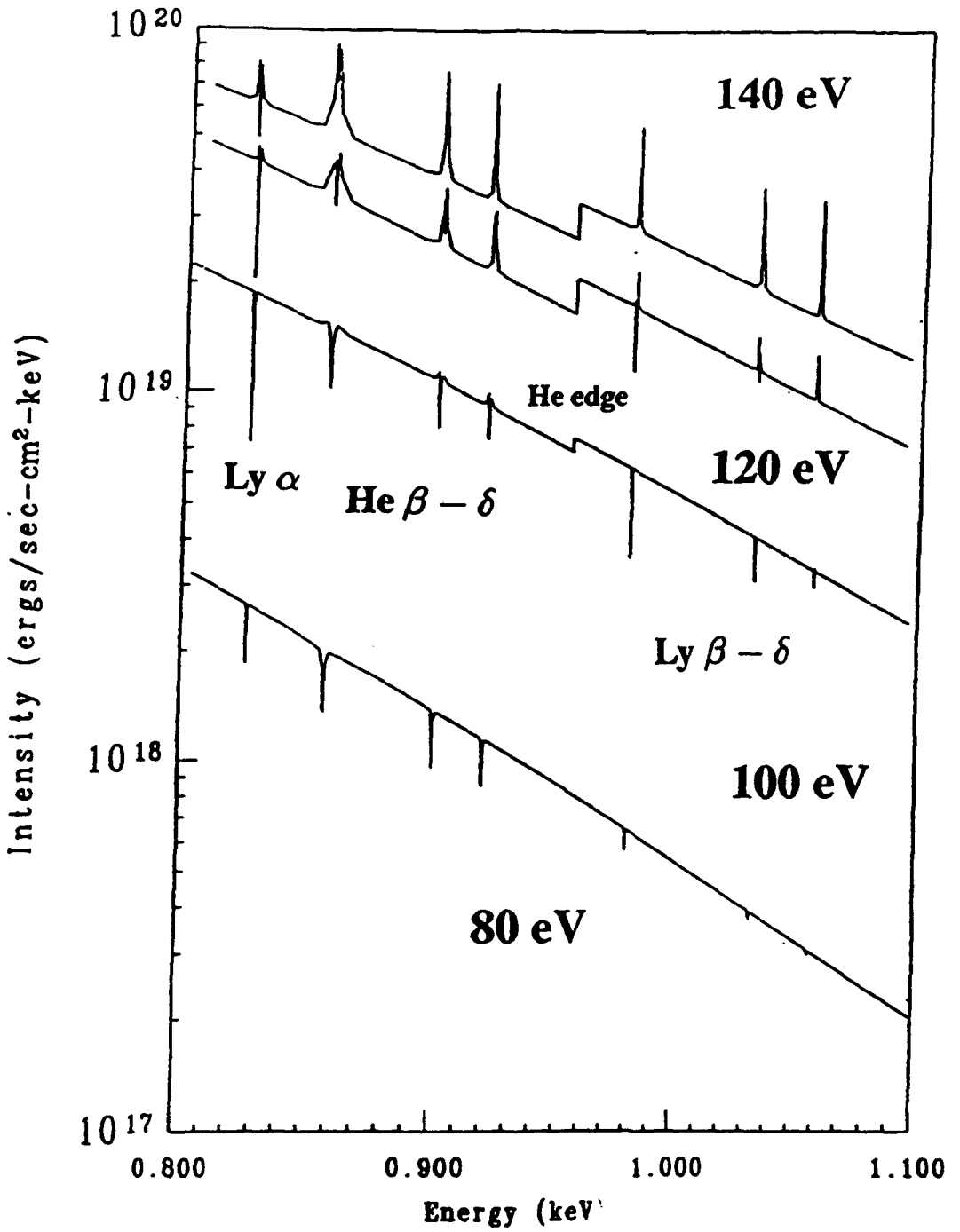

FIG. 13. Evolution of the K shell spectrum of fluorine as the temperature increases from 80 to 140 eV with the foam density fixed at 10 mg cm^{-3}.

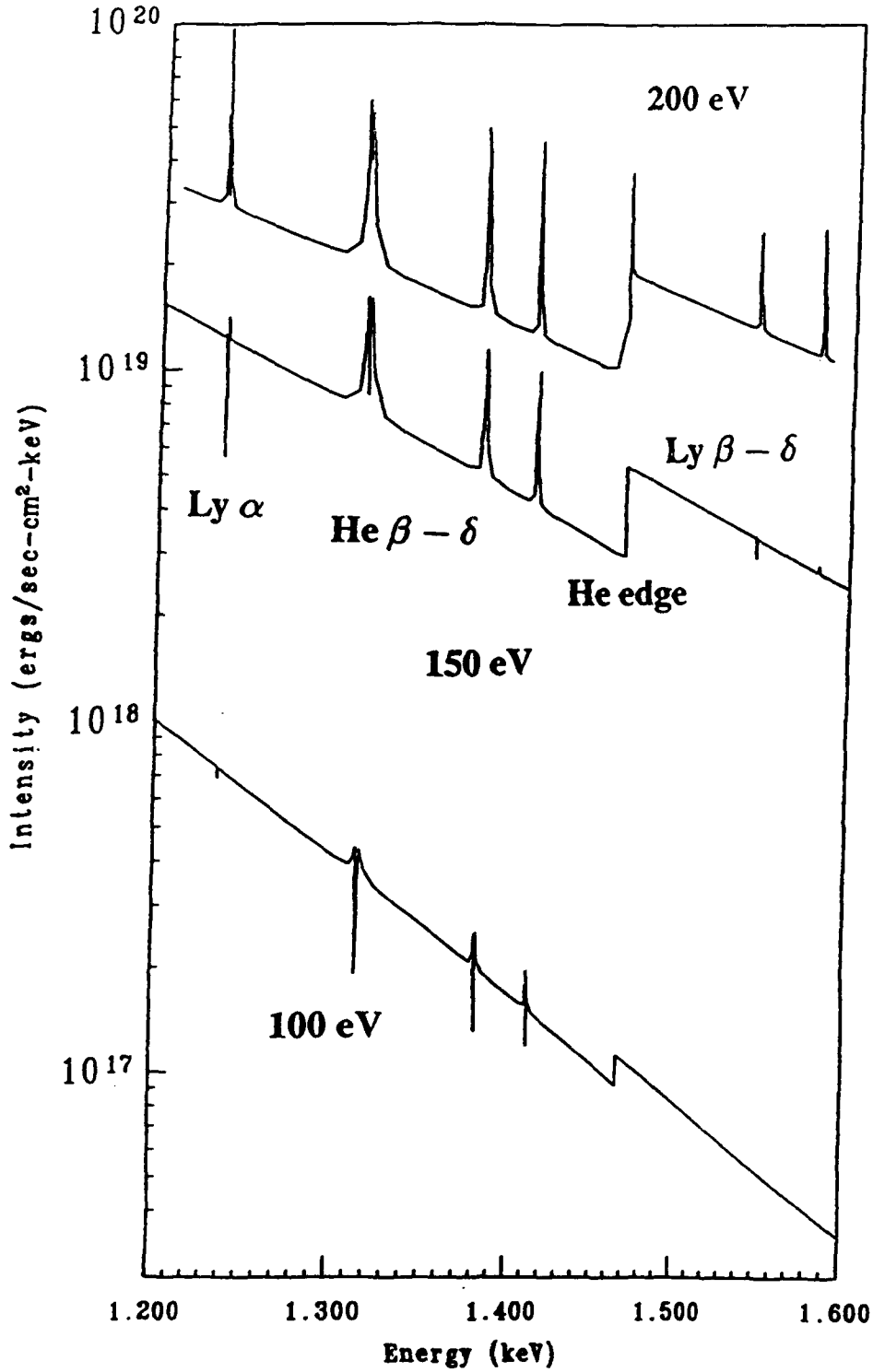

FIG. 14. The predicted K shell spectrum of the sodium dopant changes markedly as the temperature increases from 100 to 200 eV. Foam density is fixed at 10 mg cm^{-3}.

• 200 eV: The foam density of 10 mg cm^{-3} is only one-fourth of that used in the previous series of calculations. As a result, the continuum is so far below the Planck limit that all the lines are now in emission.

The principal conclusions of our study at a fixed density of 10 mg cm^{-3} are : i) temperature distinctions as fine as 10 eV may be made in the 50-100 eV regime providing that oxygen is included as a dopant along with Na and F, ii) the fluorine spectrum can differentiate the temperature in 20 eV increments from 80 eV to 140 eV, and, iii) due to the lower carbon density, the continuum falls further from the Planck limit, especially at the higher temperatures considered. The result is that most of the spectral lines are seen in emission at 150 eV, and all at 200 eV.

V. Inhomogeneous Foam Plasmas

In the initial ion-beam foam target experiments the foams expected to be used are of somewhat lower density than those considered above (i.e., about 3 mg cm^{-3} instead of 10 mg cm^{-3} or higher). Doping of these foams with tracer elements is difficult at such low densities although it is expected to be feasible eventually, and is certainly possible at higher target densities. To provide initial diagnostic predictions for these experiments we have performed calculations for the emitted spectra of foams of CH as well as $C_{12}H_{18}O_{10}$. The temperature-density profile is a more realistic non-uniform distribution from a radiation-hydrodynamics calculation, courtesy of M. K. Matzen and R. Dukart of Sandia National Laboratories. The same profile is used for both foam compositions and is illustrated in Figs. 15 and 16.

The spectra presented in Figs. 17-19 following the temperature and density plots are calculated as viewed from the low-temperature side of the foam (displacement = 0). Fig. 17 shows the entire spectrum of the CH foam. A somewhat more detailed carbon table has been used than that employed for previous calculations, allowing the higher level K shell lines to be included. Note from Fig. 17 that the lower plasma density has resulted in the spectrum falling significantly below the Planck limit, although its overall *shape* could still be credibly interpreted as Planckian. The comparison blackbody curve is for an 85 eV radiation temperature since that is the highest temperature attained in the foam plasma. Fig. 18 shows a closeup of the carbon K shell lines, with the Ly α - He γ blend the most prominent feature, and He α nearly of equal

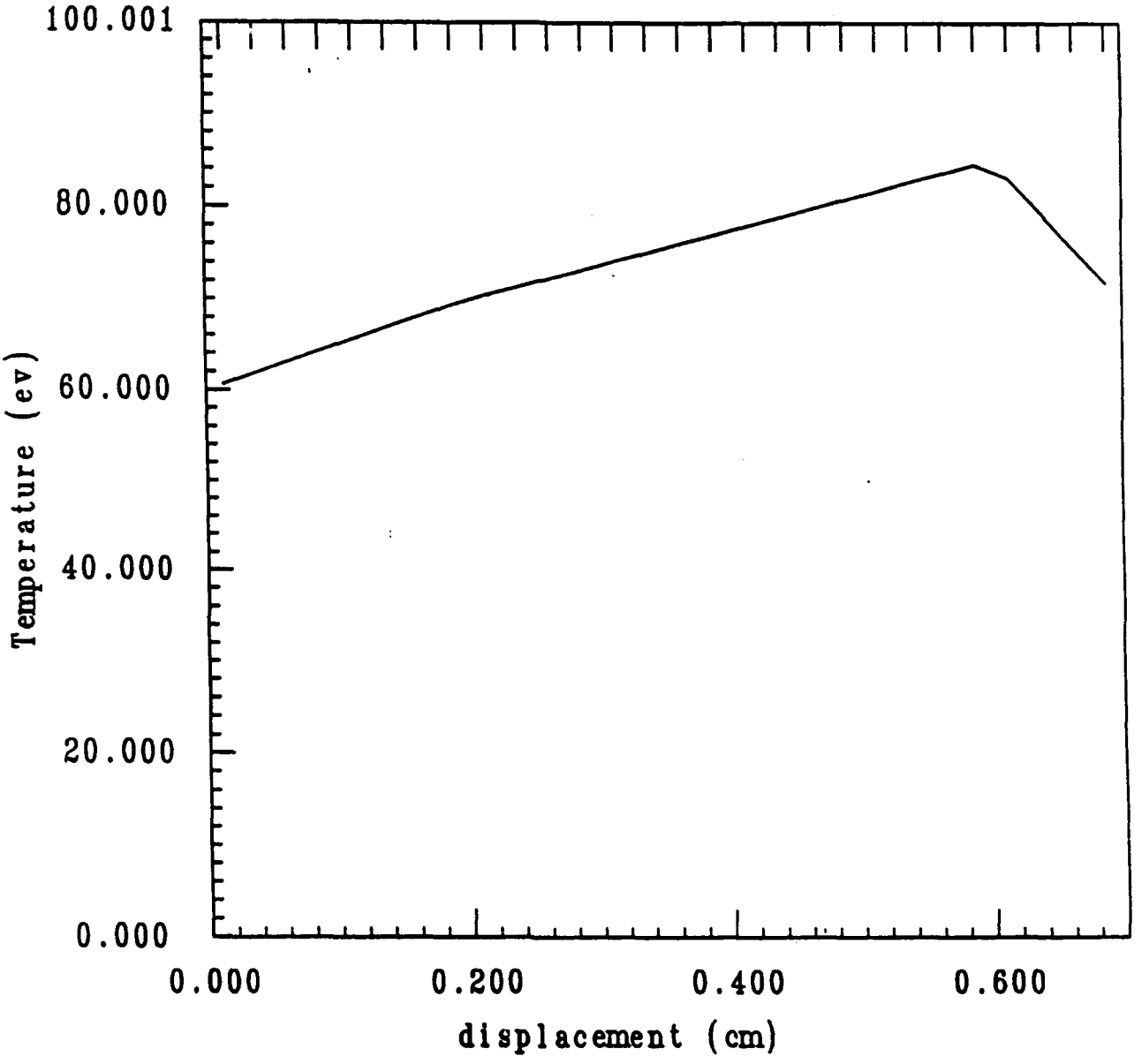

FIG. 15. Calculated temperature profile of ion beam foam target converter, courtesy of M. K. Matzen and R. Dukart of Sandia National Laboratories.

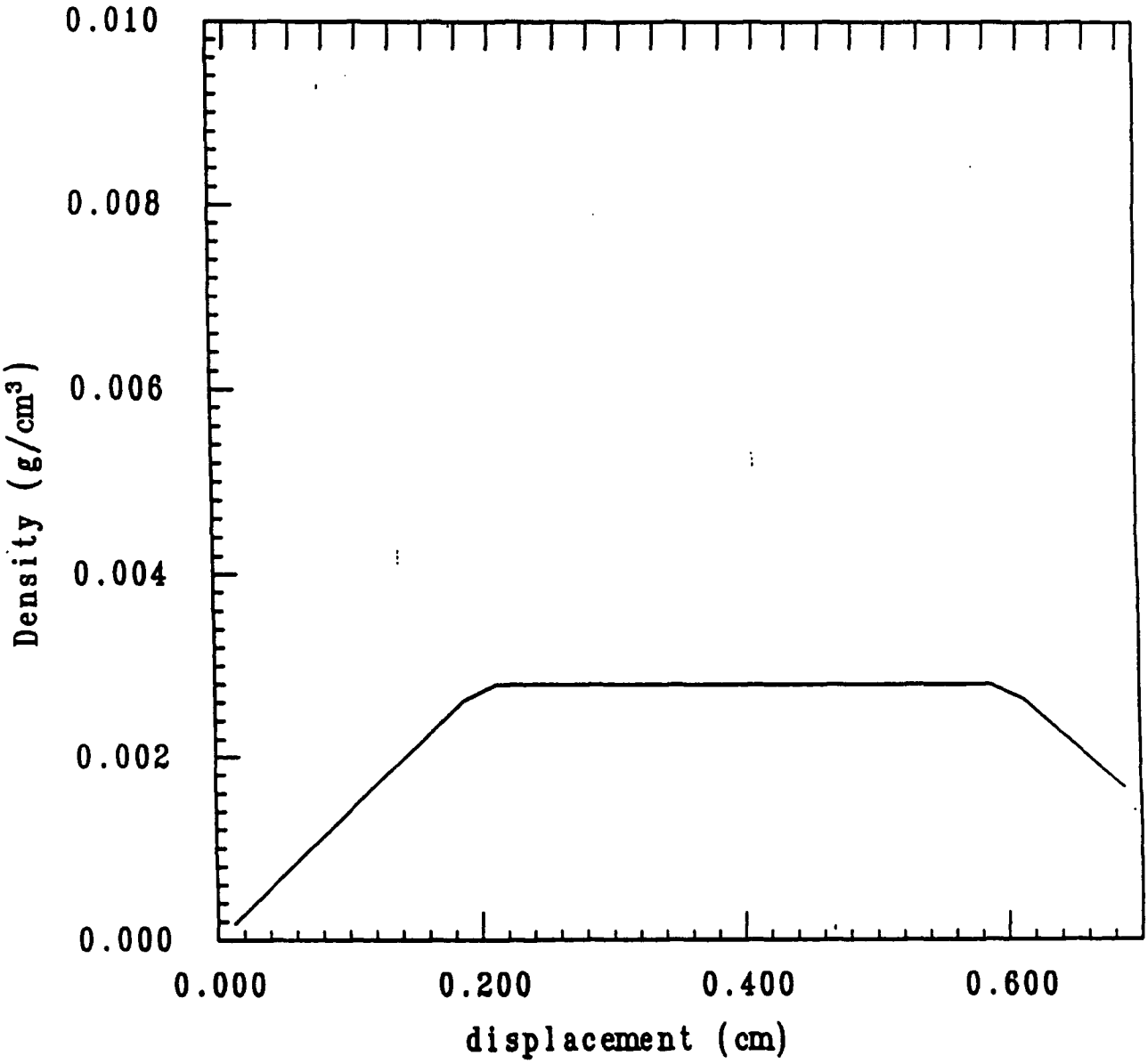

FIG. 16. Density profile of the foam target from the same calculation as in Fig. 15.

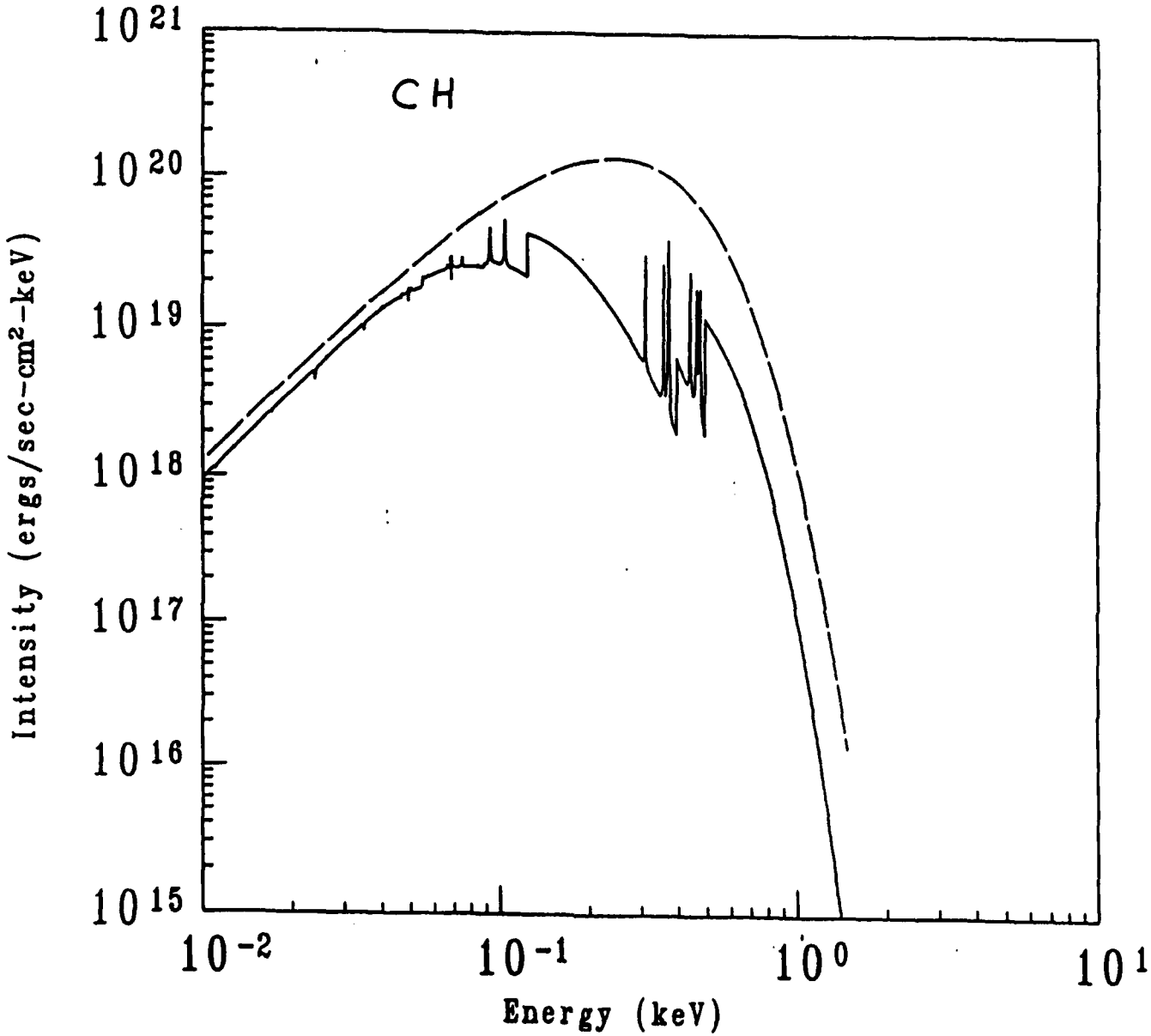

FIG. 17. Full spectrum calculated to be emitted from the foam target of Figs. 15 and 16, assuming that the composition of the foam is CH, without dopants. Spectrum is viewed from the low-temperature (displacement = 0) side of the plasma.

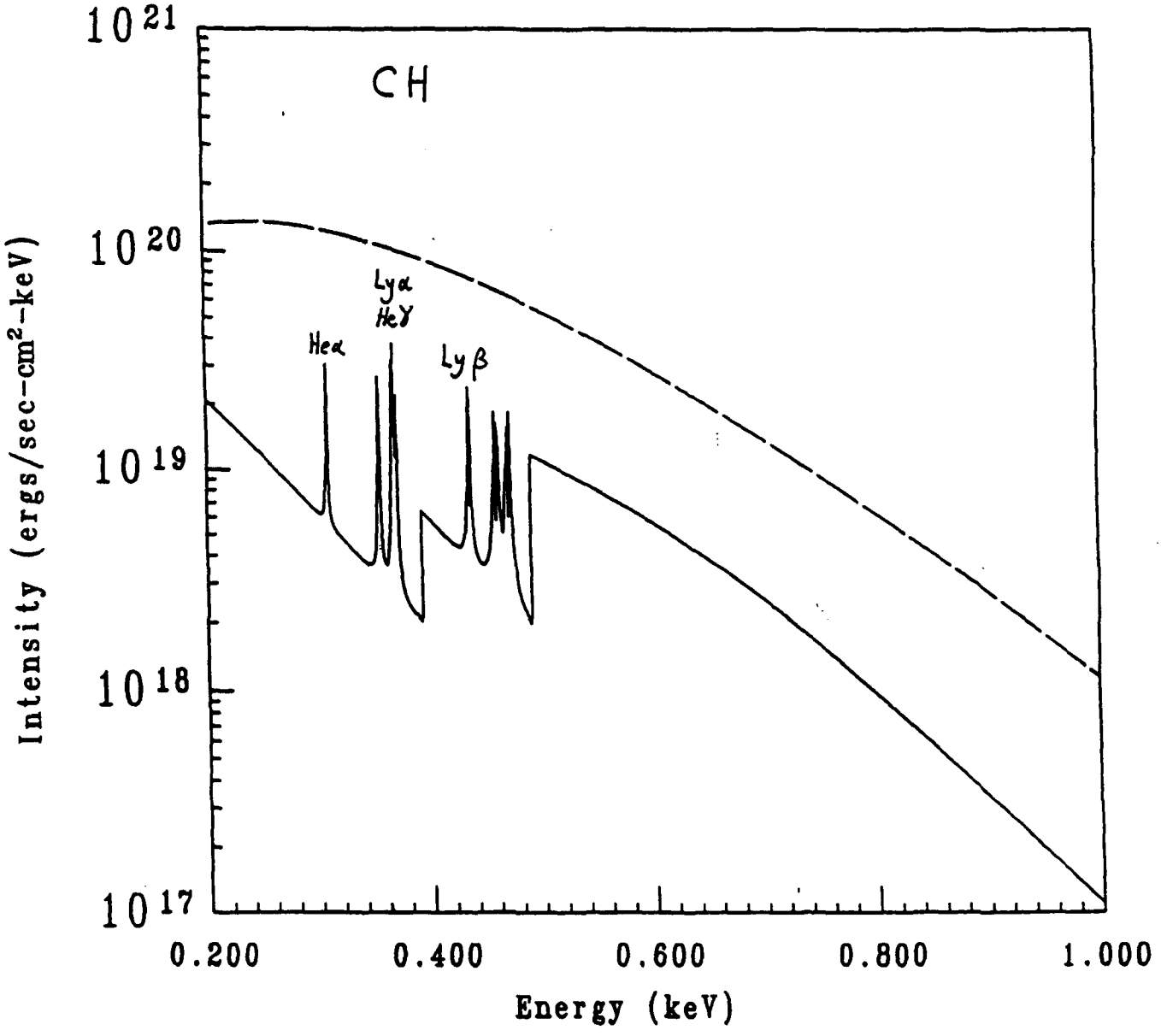

FIG. 18. Portion of the same spectrum of Fig. 17, focusing on the K shell lines of carbon.

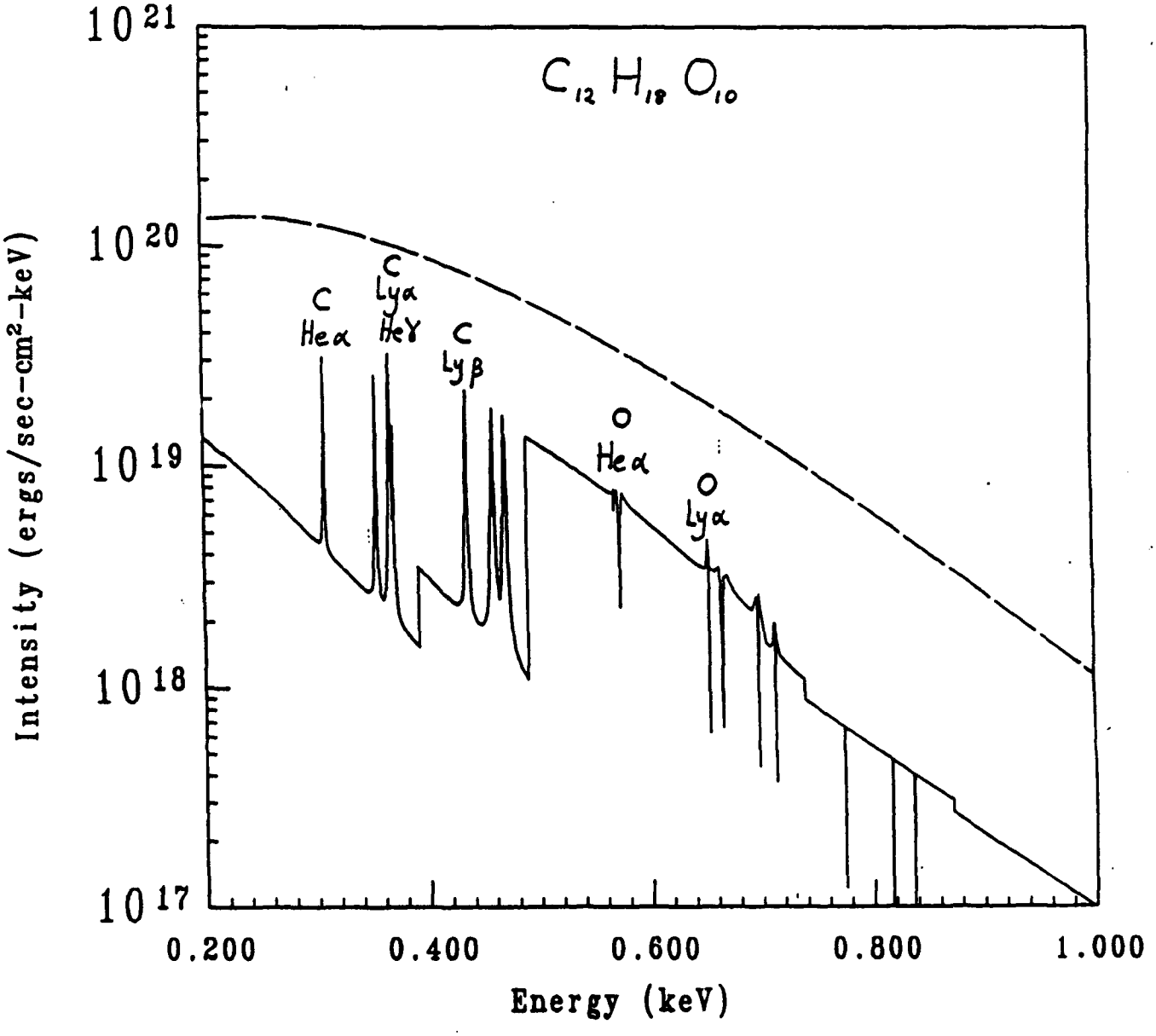

FIG. 19. As in Fig 18, except that the composition of the foam is assumed to be $C_{12}H_{18}O_{10}$.

intensity. Fig. 19 illustrates the spectrum from an oxygen-bearing foam ($C_{12}H_{18}O_{10}$) of the identical temperature-density profile as the CH case. All of the principal K shell lines of oxygen appear in absorption against the strong hydrogenic continuum emission of carbon. As with sodium and fluorine, the carbon and oxygen K lines are cleanly separated, all of the carbon lines lying below 500 eV, and the oxygen lines all above 550 eV. The strong presence of O Ly α indicates that temperatures of at least 70 eV have been attained in the target. This temperature benchmark using oxygen has also been noted above for previous calculations. Therefore, even if dopants cannot be used in a particular experiment, use of oxygen-bearing foams is recommended as a way to obtain additional diagnostic information.

VI. Simulation of Magnesium Fluoride Macrodot Experiment

In a recent experiment at Sandia, a 1μm thick target of MgF_2 (referred to as a "macrodot") was exposed to the x-rays from a Z pinch radiation source. The response of the MgF_2 target to the x-rays was observed with x-ray spectrometers[13], which were looking primarily at the Mg K shell lines. In this spectral region, the He α line was the dominant feature, and the He-like intercombination line and various satellite lines were also detected. An initial analysis[13] employed standard line ratios involving the resonance, intercombination, and satellite lines. This method suggested that temperatures of 50-70 eV had been attained, at electron densities of 10^{20} - 10^{21} cm^{-3}.

Using the multifrequency, one-dimensional version of the NRL radiation hydrodynamics model, we have simulated this experiment with the atomic data tables for Mg and F described above in Sec. II. The Z pinch source spectrum is modeled as a two-component radiation field. Both components have a Gaussian time profile, with a full-width-at-half-maximum of 15 ns. The low energy ("soft") component is taken as an undiluted 48 eV blackbody at the peak of the Gaussian. The temperature of the assumed Planckian varies such that T^4 is Gaussian. The higher energy ("hard") component is assumed to consist of photons lying entirely between 1.6 and 2.1 keV, whose intensity per unit energy interval is constant in that range. The total hard power is 120 GW cm^{-2} at the peak of the radiation pulse.

The calculation reveals that the 1μm of MgF_2 heats and expands, much like exploding foils used in x-ray laser experiments[14] or the plastic window used to retain the neon in the Sandia

sodium-neon x-ray laser targets[15]. Fig. 20 shows that a gentle temperature gradient is established by the time of the peak of the external x-ray pulse. The calculated temperature of 70-80 eV is in satisfactory agreement with the initial estimates[13] of 50-70 eV. Furthermore, the electron density as shown in Fig. 21 varies from (1-4) x 10^{20} cm^{-3}, also in good agreement with the Ref. 13 analysis. Fig. 22 shows the calculated spectrum from 0.7 to 2.0 keV, containing all the K shell lines of both F and Mg. This spectrum reveals that Mg He α is predicted to be the highest intensity line, also in agreement with experiment. This very respectable convergence on conditions using independent methods demonstrates a good understanding of the physics of the experiment as well as a useful benchmark for the model.

Finally, we note that two fundamental processes are responsible for stripping the Mg plasma. One is heating of the plasma by the radiation source, which makes the electrons hot enough to further collisionally ionize the Mg. The other is direct photoionization of the Mg ions by the radiation field. The effect of direct photoionization is shown in the calculations presented in Figs. 23 and 24, where the He-like fraction is shown as a function of temperature and density. The contours for a He-like fraction exceeding 0.9 are considerably broader in Fig. 24, where the effect of the pump field is included, than in Fig. 23, where it is not. This effect is most pronounced at the lower densities as would be expected, since collisional ionization is weaker.

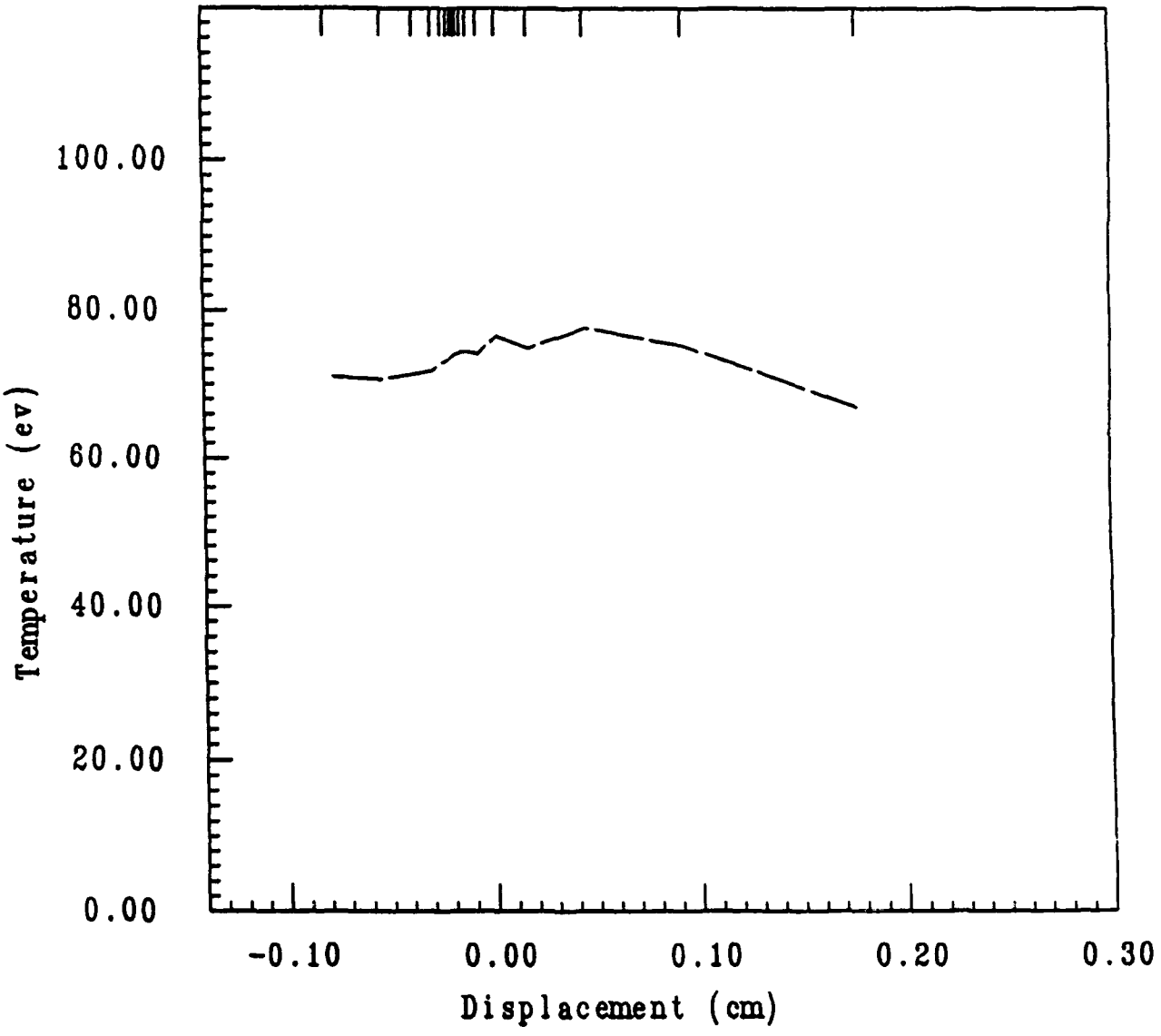

FIG. 20. Temperature of the MgF_2 "macrodot" plasma vs. position at the peak of the external heating pulse. Initial position of the target is displacement = 0.

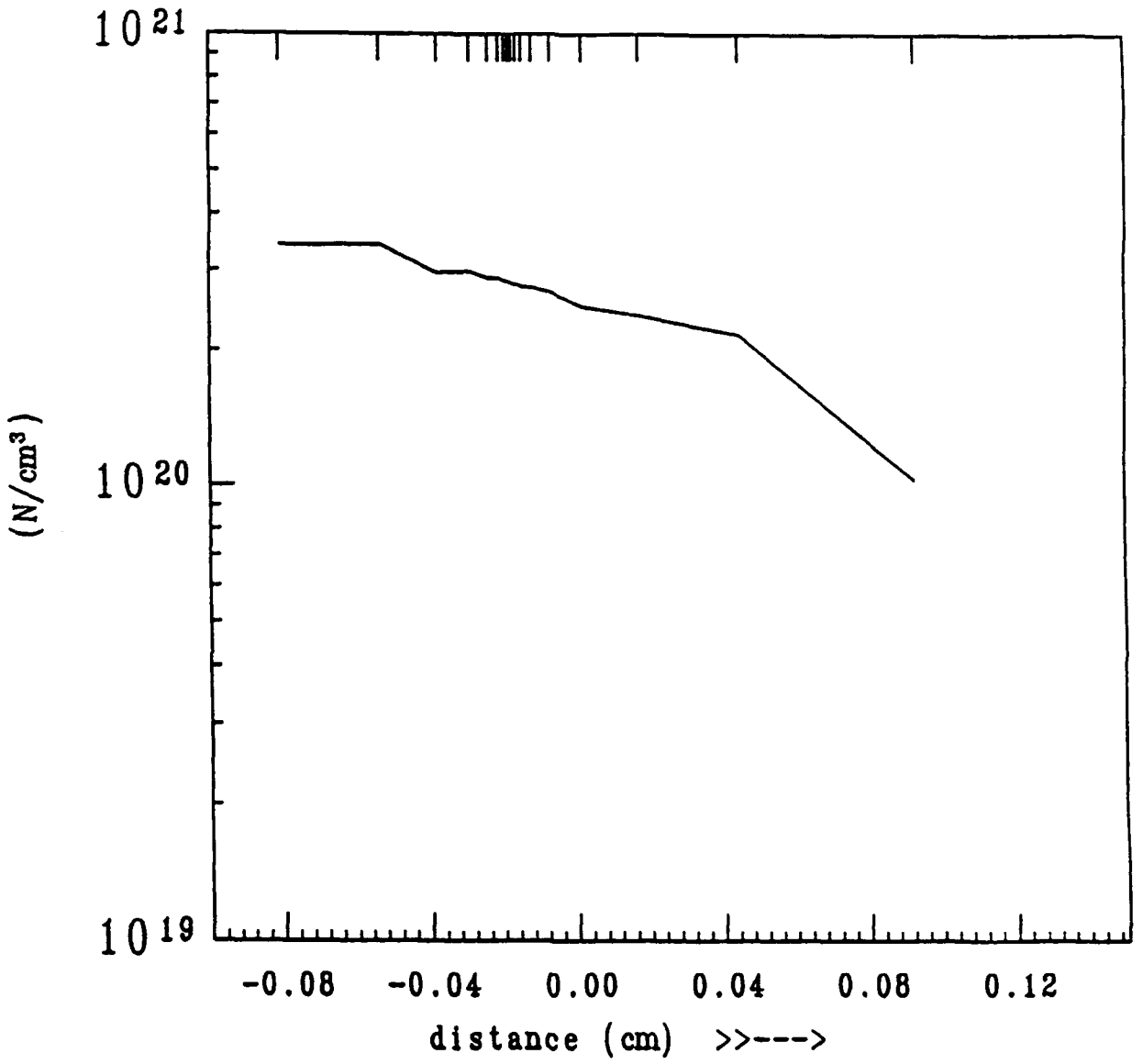

FIG. 21. As in Fig. 20, except that electron density is plotted.

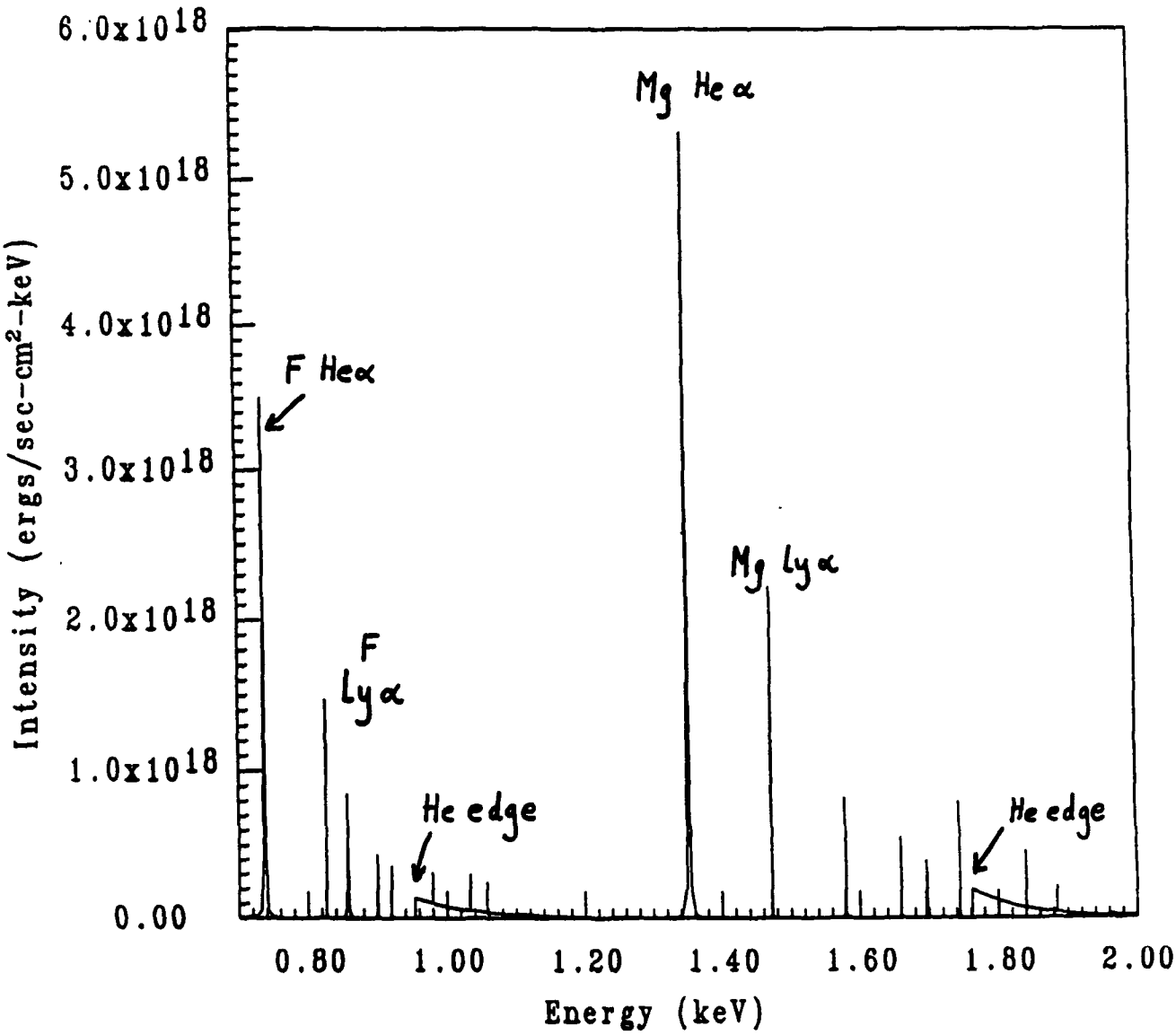

FIG. 22. Spectrum of the K shell lines of both F and Mg as calculated at the peak of the external x-ray pulse in the MgF_2 "macrodot" experiment.

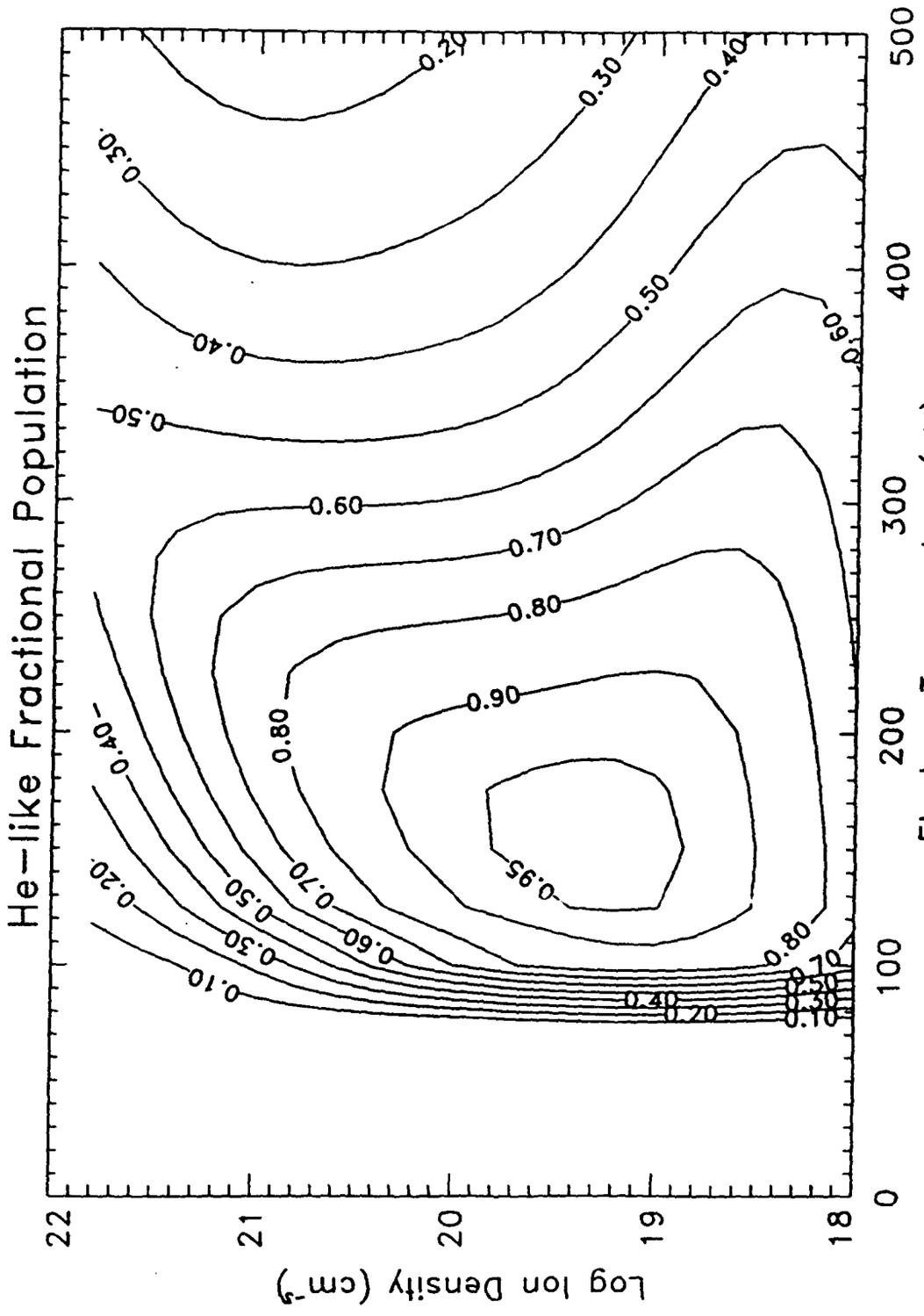

FIG. 23. He-like fraction for Mg is plotted as a function of temperature and density with no external radiation field pumping the plasma in the calculation. Collisional-radiative equilibrium is assumed.

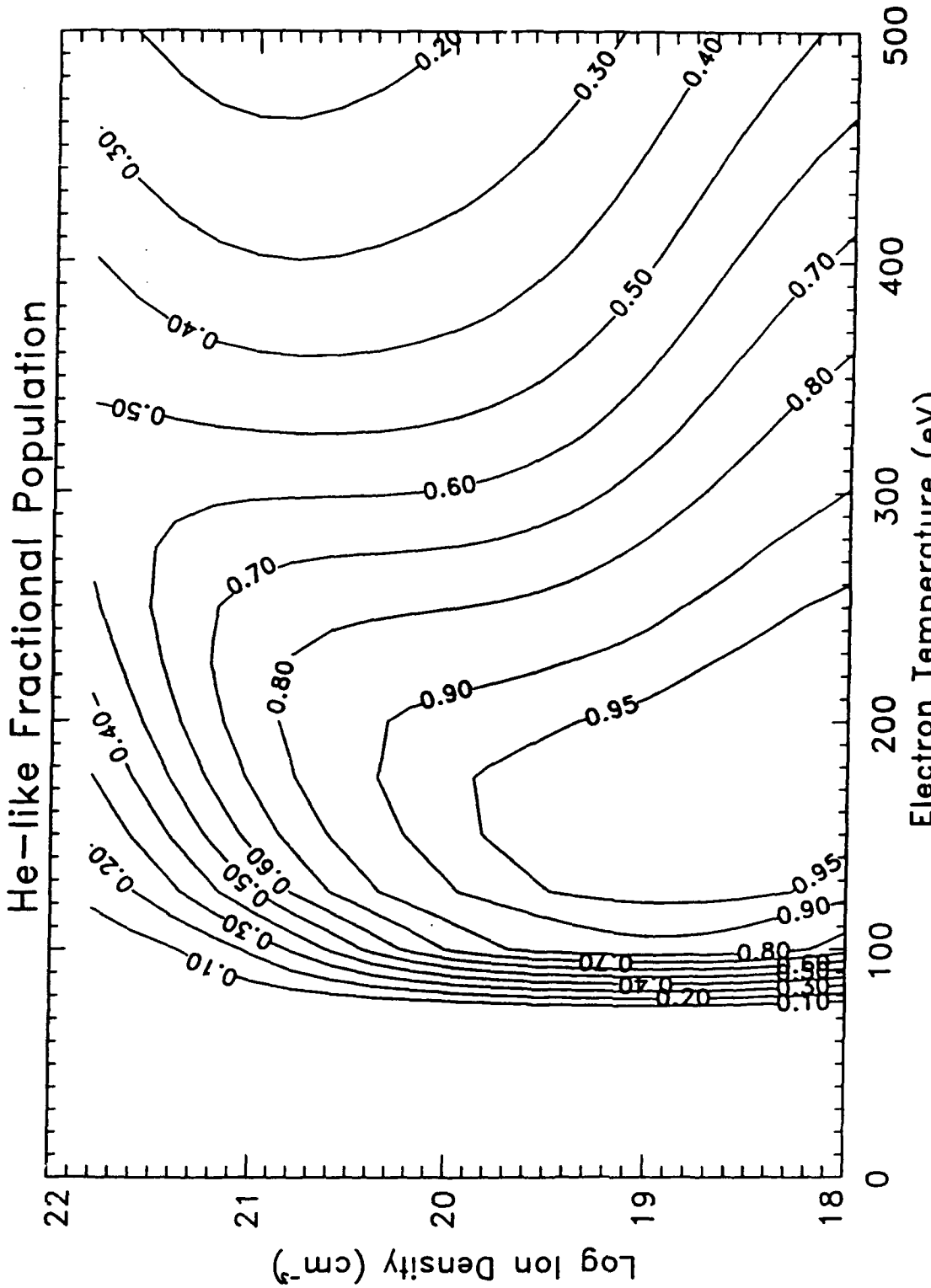

FIG. 24. As in Fig. 23, except that photoionization by the external pump radiation source discussed in Sec. VI is included in calculating the ionization balance.

VII. Acknowledgments

The authors thank M. K. Matzen of Sandia National Laboratories for innumerable valuable comments and suggestions, and J. Bailey, also of Sandia, for useful discussions on spectroscopic issues. This work was supported by Sandia National Laboratories under contract No. DC-AC04-76DP00789, purchase order AB-8449.

VIII. References

1. G. A. Chandler et al., Rev. Sci. Instrum. **63**, 4828 (1992).

2. R. W. Clark, J. Davis, and F. L. Cochran, Phys. Fluids **29**, 1971 (1986).

3. J. P. Apruzese, P. C. Kepple, K. G. Whitney, J. Davis, and D. Duston, Phys. Rev. A **24**, 1001 (1981).

4. A. Hauer, K. G. Whitney, P. C. Kepple, and J. Davis, Phys. Rev. A **28**, 963 (1983).

5. D. Duston and J. Davis, Phys. Rev. A **23**, 2602 (1981).

6. W. A. Lokke and W. H. Grasberger, **XSNQ-U - A Non-LTE Emission and Absorption Coefficient Subroutine**, Lawrence Livermore National Laboratory Report UCRL-52276 (1977).

7. A. Weiss, J. J. Keady, and N. H. Magee, At. Data Nucl. Data Tables **45**, 209 (1990).

8. W. L. Wiese, M. W. Smith, and B. M. Glennon, in **Atomic Transition Probabilities**, National Bureau of Standards Report No. NSRDS-NBS-4 (U. S. Government Printing Office, Washington DC, 1966), p. ix.

9. D. H. Sampson and H. Zhang, Astrophys. J. **335**, 516 (1988).

10. K. G. Whitney, J. Davis, and J. P. Apruzese, Phys. Rev. A **22**, 2196 (1980).

11. E. H. Avrett and D. G. Hummer, Mon. Not. R. Astron. Soc. **130**, 295 (1965).

12. R. H. Marjoribanks, M. C. Richardson, P. A. Jaanimagi, and R. Epstein, Phys. Rev. A **46**, R1747 (1992).

13. J. Bailey (Sandia National Laboratories), private communication (1992).

14. R. A. London and M. D. Rosen, Phys. Fluids **29**, 3813 (1986).

15. J. L. Porter, R. B. Spielman, M. K. Matzen, E. J. McGuire, L. E. Ruggles, M. F. Vargas, J. P. Apruzese, R. W. Clark, and J. Davis, Phys. Rev. Lett. **68**, 796 (1992).